van Doorn, P.A., Ruts, L., Jacobs, B.C., 2008. Clinical features, pathogenesis, and treatment of Guillain–Barré syndrome. Lancet Neurol. 7, 939–950.
Vernino, S., Sandroni, P., Singer, W., Low, P.A., 2008. Invited article: autonomic ganglia: target and novel therapeutic tool. Neurology 70, 1926–1932.
Windebank, A.J., Blexrud, M.D., Dyck, P.J., Daube, J.R., Karnes, J.L., 1990. The syndrome of acute sensory neuropathy: clinical features and electrophysiologic and pathologic changes. Neurology 40, 584–591.
Yamashita, F., Hirayama, M., Nakamura, T., Takamori, M., Hori, N., Uchida, K., Hama, T., Sobue, G., 2010. Pupillary autonomic dysfunction in multiple system atrophy and Parkinson's disease: an assessment by eye-drop tests. Clin. Auton. Res. 20, 191–197.
Zochodne, D.W., 1994. Autonomic involvement in Guillain–Barré syndrome: a review. Muscle Nerve 17, 1145–1155.

Brain Advance Access published July 26, 2013

doi:10.1093/brain/awt183 Brain 2013: Page 1 of 12 | 1

BRAIN
A JOURNAL OF NEUROLOGY

Positive feedback loop via astrocytes causes chronic inflammation in virus-associated myelopathy

Hitoshi Ando,[1] Tomoo Sato,[1] Utano Tomaru,[2] Mari Yoshida,[3] Atae Utsunomiya,[4] Junji Yamauchi,[1] Natsumi Araya,[1] Naoko Yagishita,[1] Ariella Coler-Reilly,[1] Yukiko Shimizu,[1] Kazuo Yudoh,[5] Yasuhiro Hasegawa,[6] Kusuki Nishioka,[7] Toshihiro Nakajima,[7] Steven Jacobson[8] and Yoshihisa Yamano[1]

1 Department of Rare Diseases Research, Institute of Medical Science, St. Marianna University School of Medicine, Kanagawa, Japan
2 Department of Pathology, Hokkaido University Graduate School of Medicine, Sapporo, Japan
3 Institute for Medical Science of Ageing, Aichi Medical University, Aichi, Japan
4 Department of Haematology, Imamura Bun-in Hospital, Kagoshima, Japan
5 Institute of Medical Science, St. Marianna University School of Medicine, Kanagawa, Japan
6 Department of Neurology, St. Marianna University School of Medicine, Kanagawa, Japan
7 Institute of Medical Science, Tokyo Medical University, Tokyo, Japan
8 Viral Immunology Section, Neuroimmunology Branch, National Institutes of Health, Bethesda, MD, USA

Correspondence to: Yoshihisa Yamano, MD, PhD
Department of Rare Diseases Research,
Institute of Medical Science,
St. Marianna University School of Medicine,
2-16-1, Sugao, Miyamae-ku,
Kawasaki 216-8512,
Japan
E-mail: yyamano@marianna-u.ac.jp

Human T-lymphotropic virus type 1-associated myelopathy/tropical spastic paraparesis (HAM/TSP) is a rare neurodegenerative disease characterized by chronic inflammation in the spinal cord. We hypothesized that a positive feedback loop driven by chemokines may be responsible for the chronic inflammation in HAM/TSP. We aimed to determine the identity of these chemokines, where they are produced, and how they drive chronic inflammation in HAM/TSP. We found that patients with HAM/TSP have extraordinarily high levels of the chemokine CXCL10 (also known as IP-10) and an abundance of cells expressing the CXCL10-binding receptor CXCR3 in the cerebrospinal fluid. Histological analysis revealed that astrocytes are the main producers of CXCL10 in the spinal cords of patients with HAM/TSP. Co-culture of human astrocytoma cells with $CD4^+$ T cells from patients with HAM/TSP revealed that astrocytes produce CXCL10 in response to IFN-γ secreted by $CD4^+$ T cells. Chemotaxis assays results suggest that CXCL10 induces migration of peripheral blood mononuclear cells to the central nervous system and that anti-CXCL10 neutralizing antibody can disrupt this migration. In short, we inferred that human T-lymphotropic virus type 1-infected cells in the central nervous system produce IFN-γ that induces astrocytes to secrete CXCL10, which recruits more infected cells to the area via CXCR3, constituting a T helper type 1-centric positive feedback loop that results in chronic inflammation.

Keywords: HTLV-1; HAM/TSP; CXCL10; CXCR3; astrocyte

Abbreviation: HAM/TSP = human T-lymphotropic virus type 1-associated myelopathy/tropical spastic paraparesis

Received February 18, 2013. Revised May 3, 2013. Accepted May 26, 2013.

Introduction

The rise of chronic inflammatory disorders has prompted researchers to reconsider the classical concept of inflammation, which dates back to ancient Roman times when inflammation was first defined as redness, swelling, heat and pain in response to injury or infection. In general, inflammation is an adaptive immune response to tissue malfunction that ideally neutralizes the source of the disturbance and restores tissue homeostasis. Paradoxically, a prolonged state of inflammation has been implicated in the pathogenesis of various diseases characterized by the loss of homeostasis, such as autoimmune diseases, cancers and neurodegenerative diseases (Libby, 2002; Mantovani *et al.*, 2008; Medzhitov, 2008, 2010). To produce effective therapies for these debilitating disorders, we must first elucidate the mechanisms by which this maladaptive chronic inflammatory state develops.

Although there are many chronic inflammatory disorders for which the initiating trigger is ill-defined or unknown, human T-lymphotropic virus type 1 (HTLV-1)-associated myelopathy/tropical spastic paraparesis (HAM/TSP) is a rare neurodegenerative chronic inflammatory disease clearly caused by HTLV-1 retroviral infection (Gessain *et al.*, 1985; Osame *et al.*, 1986). In other words, the HTLV-1-infected cells in patients with HAM/TSP represent a useful starting point from which to investigate the origins of chronic inflammation.

HTLV-1 infects 10–20 million people worldwide, some of whom develop serious conditions such as adult T cell leukaemia (Hinuma *et al.*, 1981) and up to 2–3% of whom develop the debilitating inflammation in the spinal cord that characterizes HAM/TSP (Gessain *et al.*, 1985; Osame *et al.*, 1986). Evidence has accumulated to support the theory that infected $CD4^+$ T cells (as opposed to infected neuronal cells or non-infected peripheral blood mononuclear cells) are primarily responsible for this transition to the HAM/TSP disease state: HTLV-1 primarily infects $CD4^+$ T cells (Richardson *et al.*, 1990); levels of infected $CD4^+$ T cells circulating in the blood of patients with HAM/TSP are higher than those in the blood of asymptomatic carriers (Nagai *et al.*, 1998; Yamano *et al.*, 2002), the levels in the CSF surrounding the spinal cord are higher still (Nagai *et al.*, 2001*a*); and these infected $CD4^+$ T cells have also been detected in the spinal cord lesions themselves (Moritoyo *et al.*, 1996; Matsuoka *et al.*, 1998). There are many cell types capable of producing an inflammatory response upon contact with viral antigens, and it is true that the cases where these antigen-specific cells are most abundant are indeed in patients with HAM/TSP, but there is a large range of overlap in which patients with HAM/TSP and asymptomatic carriers have the same amount of antigen-specific cells in their peripheral blood mononuclear cells (Jacobson *et al.*, 1990; Jeffery *et al.*, 1999; Kubota *et al.*, 2000; Yamano *et al.*, 2002). Therefore, we hypothesized that their presence may not be the key factor that determines a patient's fate to experience the disease or not, and that perhaps there might be another cell type responsible for initiating the chronic inflammation in HAM/TSP through a more unique pathway. Research shows that infected $CD4^+$ T cells are indeed capable of migrating across the blood–brain barrier into the CNS (Furuya *et al.*, 1997) and secreting proinflammatory cytokines such as interferon-gamma (IFN-γ) (Hanon *et al.*, 2001; Yamano *et al.*, 2005, 2009). We guessed that these cells might even be capable of producing IFN-γ spontaneously due only to intracellular activation of transcription factors by the invading HTLV-1 virus, which has been shown to be capable of such potent effects (Waldmann, 2006).

Studies have indicated that among the $CD4^+$ T cell subtypes, immune responses by $CD4^+$ T helper type 1 (Th1)-like cells may be dominant in patients with HAM/TSP (Goon *et al.*, 2002; Narikawa *et al.*, 2005), leading to the theory that the Th1 axis should be the primary focus in the study of HAM/TSP. These Th1 cells express both the CC chemokine receptor type 5 (CCR5) and CXC motif receptor 3 (CXCR3), which respond to the presence of CC motif ligand (CCL) 3, 4 and 5 and CXC motif ligand (CXCL) 9, 10 and 11, respectively. These ligands are chemokines, a subclass of cytokines that stimulate directed chemotaxis in responsive cells, and it is known that chemokine receptor–ligand interactions play an important role in recruiting immune cells to inflammatory sites (Luster, 1998; Qin *et al.*, 1998). Of particular interest are the CXCR3 agonists, which are regulated by the aforementioned proinflammatory cytokine IFN-γ and carry this relationship in the alternative nomenclature: monokine induced by gamma interferon (MIG/CXCL9), IFN-γ-inducible protein 10 (IP-10/CXCL10), and interferon-inducible T cell alpha chemoattractant (I-TAC/CXCL11) (Proost *et al.*, 2001, 2003). We and others have shown that CCL5, CXCL9, and especially CXCL10, are elevated in the CSF of patients with HAM/TSP (Teixeira *et al.*, 2004; Narikawa *et al.*, 2005; Tanaka *et al.*, 2008; Sato, in press).

We hypothesized that these chemokines play a key role in the pathogenesis of HAM/TSP by recruiting more cells infected with HTLV-1 to the inflammation site and potentially initiating a positive feedback loop. We first compared the levels of several chemokines in the serum and CSF of patients with HAM/TSP and asymptomatic carriers and found that CXCL10 was the most closely associated with known features of HAM/TSP pathogenesis, namely increased CSF cell count. We then analysed samples of peripheral blood mononuclear cells and CSF cells along with images of the spinal cord tissue to demonstrate that $CD4^+$ cells expressing CXCL10-binding CXCR3, namely cells of the Th1 subtype, are indeed infected with HTLV-1, do migrate across the blood–brain barrier into the CNS, and do produce IFN-γ in patients with HAM/TSP. We demonstrated that this IFN-γ production can occur in the absence of external stimuli. Immunohistochemical analysis of the spinal cord tissue not only confirmed that CXCL10 production is elevated in patients with HAM/TSP but also revealed that astrocytes may be the main producers of CXCL10 in the spinal cord. We used novel techniques to demonstrate that these astrocytes likely represent the missing piece of the puzzle in the positive feedback loop: infected $CD4^+$ T cells produce IFN-γ, which stimulates astrocytes to produce CXCL10, which recruits more $CD4^+CXCR3^+$ Th1 cells to the CNS. Finally, chemotaxis assays were used to compare the inhibitory potentials of anti-CXCL10 and anti-CXCR3 neutralizing antibodies on this positive feedback loop as the first step toward the development of an effective therapy.

Materials and methods

Patient selection and sample preparation

Written informed consent was obtained from all patients before the study, which was reviewed and approved by the Institutional Ethics Committee (St. Marianna University) and conducted in compliance with the tenets of the Declaration of Helsinki. The study included 26 HTLV-1 non-infected healthy donors (14 females and 12 males; mean age, 49 years), 29 asymptomatic carriers (21 females and eight males; mean age, 50 years), 17 patients with adult T cell leukaemia with no history of chemotherapy (eight females and nine males; mean age, 68 years), and 58 patients with HAM/TSP (47 females and 12 males; mean age, 62 years). Diagnosis of adult T cell leukaemia was based on the criteria established by Shimoyama (1991). HTLV-1 seropositivity was determined by a particle agglutination assay (Serodia-HTLV-1) and confirmed by western blot (SRL Inc.). HAM/TSP was diagnosed according to WHO guidelines (Osame, 1990).

Samples of peripheral blood mononuclear cells were prepared using density gradient centrifugation (Pancoll; PAN-Biotech) and viably cryopreserved in liquid nitrogen with freezing medium (Cell Banker 1; Mitsubishi Chemical Medience Corporation). Plasma and serum samples were obtained from 16 healthy donors, 26 asymptomatic carriers, 30 patients with HAM/TSP and 14 patients with adult T cell leukaemia (six smouldering type and eight chronic type). Multiple serum and CSF samples were taken within a 1-h window for each of 32 patients with HAM/TSP. A Fuchs–Rosenthal chamber (Hausser Scientific Company) was used for CSF cell counts, after which the cells were isolated by centrifugation and cryopreserved in the aforementioned freezing medium. A medulla oblongata tissue sample from one patient with HAM/TSP as well as thoracic spinal cord tissues from four patients with HAM/TSP and six control individuals with no spinal cord lesions (numbered controls 1–6; one female and five males; mean age, 67 years) were obtained post-mortem, fixed in 10% formalin, and embedded in paraffin. Clinical characteristics of the patients with HAM/TSP who underwent post-mortem examination are shown in Supplementary Table 1.

Cell culture

Before culture, peripheral blood mononuclear cells from patients with HAM/TSP, asymptomatic carriers and healthy donors were sorted using MACS beads (Miltenyi Biotec) according to the manufacturer's instructions; $CD4^+$ T cells and $CD8^+$ T cells were separated negatively, and $CD14^+$ cells were separated positively, and the purity of all cell populations exceeded 95%. The isolated cells were seeded at 1×10^5 cells/200 µl/well in 96-well round-bottom plates in RPMI 1640 medium (Wako Pure Chemical Industries Ltd.) supplemented with 10% heat-inactivated human serum (Wako Pure Chemical Industries Ltd.), and 1% penicillin/streptomycin antibiotic solution (Wako Pure Chemical Industries Ltd.) without any stimuli. The culture supernatants were collected after incubating at 37°C for 24, 48 and 72 h in 5% CO_2.

U251 human astrocytoma cells were cultured in Dulbecco's minimal essential medium (Wako Pure Chemical Industries Ltd.) supplemented with 10% heat-inactivated foetal bovine serum (Gibco-Invitrogen) and 1% penicillin/streptomycin. In total, 2×10^4 U251 cells were then co-cultured in 48-well flat-bottom plates at 37°C for 48 h in 5% CO_2 with 0, 2×10^2, 2×10^3 or 2×10^4 $CD4^+$ T cells isolated from peripheral blood mononuclear cells of patients with HAM/TSP or healthy donors using MACS beads. A control group of 2×10^4 $CD4^+$ T cells was single-cultured under the same conditions. The U251 cells were also cultured with and without 1 ng/ml recombinant human IFN-γ (285-IF, R&D Systems). After culture for 48 h, $CD4^+$ T cells were removed by washing with PBS and the U251 cells were then cultured for an additional 24 h before collecting the culture supernatants.

For the experiment investigating the inhibitory potential of neutralizing antibodies, 2×10^4 $CD4^+$ T cells isolated from peripheral blood mononuclear cells of patients with HAM/TSP using MACS beads were cultured in 96-well round-bottom plates for 72 h under the same conditions, and the culture supernatant was collected after centrifugation. Then, in this supernatant, 2×10^4 U251 cells were cultured in 48-well flat-bottom plates with 10 µg/ml monoclonal neutralization antibodies: anti-IFN-γ antibody (MAB285, R&D Systems), anti-tumour necrosis factor (TNF)-α antibody (MAB610, R&D Systems), or isotype control antibody (MAB002 and MAB003, R&D Systems). The U251 cells were cultured for additional 24 h before collecting the culture supernatants for assay.

Measurement of chemokines, IFN-γ, IL-17A and sIL-2 receptor

The concentrations of four chemokines (CCL4, CCL5, CXCL9 and CXCL10) in the serum and CSF samples and levels of CXCL10, IFN-γ and IL-17A in the culture supernatants were measured with a cytometric bead array kit (BD Biosciences) using a FACSCalibur flow cytometer (BD Biosciences) according to the manufacturer's instructions. It should be noted that the cytometric bead array kit measures the total concentrations of all chemokine isoforms irrespective of aminoterminal variation (Proost *et al.*, 2001, 2003). The sIL-2R in the serum was measured using an ELISA (Cell-free N IL-2R, Kyowa Medex).

Flow cytometric analysis

Peripheral blood mononuclear cells and CSF cells, which were obtained on the same day, were immunostained with various combinations of the following fluorescence-conjugated antibodies: anti-CD3 (UCHT1), anti-CD4 (OKT4), anti-CD8 (RPA-T8), anti-CD19 (HIB19), anti-CD14 (61D3) (all from eBioscience), and anti-CXCR3 (1C6; BD Biosciences). The cells were stained with a saturating concentration of antibody in the dark (4°C, 30 min) and washed twice before analysis using FACSCalibur (BD Biosciences). Data were processed using FlowJo software (TreeStar). For cell sorting, JSAN (Bay Bioscience,) was used, and the purity exceeded 95%.

Real-time polymerase chain reaction

The HTLV-1 proviral DNA load was measured using ABI Prism 7500 SDS (Applied Biosystems) as described previously (Yamano *et al.*, 2002). In brief, DNA was extracted and 100 ng samples were analysed per well. The proviral DNA load was calculated using the following formula: copy number of HTLV-1 (*pX*) per 100 cells = (copy number of *pX*) / (copy number of β-actin / 2) × 100.

Tissue staining

Formalin-fixed thoracic spinal cord and medulla oblongata tissue sections were deparaffinized in xylene and rehydrated in a series of

graded alcohols and distilled water. The antigenicity of the tissue sections was recovered using a standard microwave heating technique. For immunohistochemistry, the slides were incubated with anti-CXCL10/IP-10 antibody, followed by detection with streptavidin–biotin–horseradish peroxidase and diaminobenzidine (DakoCytomation Japan Co. Ltd.). The $CXCL10^+$ cells in the spinal cord were also counted under the microscope; the data show the mean number of cells in three random 1-mm^2 fields per sample. Haematoxylin and eosin staining was conducted to detect inflammatory cells that had invaded the tissue samples. For immunofluorescence (thoracic spinal cord sections only), the slides were incubated in phosphate-buffered saline with 10% goat serum for 1 h at room temperature, in anti-CXCR3 antibody (Abcam), anti-CXCL10/IP-10 antibody (Santa Cruz Biotechnology), and anti-glial fibrillary acidic protein (GFAP) antibody (DakoCytomation Japan Co. Ltd) overnight at 4°C, labelled with Alexa Fluor® 488 or Alexa Fluor® 594 conjugated secondary antibody (Invitrogen), and examined under a fluorescence microscope (Nikon eclipse E600 with fluorescence filter Nikon F-FL; Nikon Instech) with rabbit or mouse immunoglobulin G (IgG) as the negative control.

Chemotaxis assay

Peripheral blood mononuclear cells from patients with HAM/TSP were washed and then suspended (at 1×10^7 cells/ml) in 37°C serum-free RPMI 1640 medium containing 1 mg/ml bovine serum albumin (Wako Pure Chemical Industries, Ltd.), hereafter 'chemotaxis medium'. The lower wells of a 96-well chemotaxis chamber (MBA96; Neuroprobe) were filled with chemotaxis medium containing 0.25 μg/ml recombinant human CXCL10 protein (266-IP; R&D Systems). For the negative control, the lower wells were filled with only the chemotaxis medium. For chemotaxis assays using neutralizing monoclonal antibodies, peripheral blood mononuclear cells were pretreated (room temperature, 30 min) with 10 μg/ml of anti-CXCL10 antibody (MAB266; R&D Systems), 10 μg/ml of anti-CXCR3 antibody (MAB160; R&D Systems), or 10 μg/ml of isotype control antibody (MAB002; R&D Systems). A polyvinylpyrrolidone-free micropore polycarbonate filter (PFD5; Neuroprobe) with 5-μm pores was placed over the lower chamber. The upper wells were filled with 1×10^6 peripheral blood mononuclear cells in 100 μl of chemotaxis medium. The chamber was incubated for 120 min at 37°C in a humidified 5% CO_2 atmosphere. After incubation, the fluid in the lower chambers was collected and cell counts were determined using FACSCalibur. To compare results across all chemotaxis assays, a chemotactic index was calculated using the following formula (Nie et al., 2009):

$$\text{Chemotactic index} = (\text{number of migrated cells in a test sample well})/(\text{number of migrated cells in a negative control well})$$

To determine the inhibitory effect of neutralizing antibodies, an inhibitory efficiency scale was calculated using the following formula:

$$\text{Inhibitory efficiency (\% inhibition)} = \{[(\text{chemotactic index of isotype control}) - 1] - [(\text{chemotactic index of neutralizing antibody}) - 1]\}/[(\text{chemotactic index of isotype control}) - 1] \times 100$$

Proliferation assay

The migrated cells in the lower chamber after the chemotaxis assay were collected and washed with RPMI 1640 medium supplemented with 5% foetal bovine serum and 1% penicillin/streptomycin. Those cells were then plated on 96-well round-bottom plates and cultured in the same medium without any mitogenic stimuli in 5% CO_2 at 37°C. Cell proliferation was measured using a ^{3}H-thymidine incorporation assay as described previously (Yamano et al., 2009).

Statistical analysis

Correlation analysis was assessed using Spearman's rank test. The paired *t*-test was used for within-group comparisons, and the *t*-test or the Mann–Whitney U-test was used for comparisons between groups. One-way ANOVA was used for multiple comparisons followed by Tukey's test. The Friedman test was used for paired multiple comparisons, followed by the Dunn test. Statistical analyses and graphs were performed using Graphpad Prism 5 and Prism statistics (GraphPad Software, Inc), and statistical significance was set at $P < 0.05$.

Results

Significantly higher levels of cerebrospinal fluid CXCL10 compared with serum CXCL10 in patients with HAM/TSP

To determine whether the aforementioned chemokines were involved in the migration of cells to the CNS, we first compared the levels of these chemokines with CSF cell counts in patients with HAM/TSP ($n = 29$). CSF cell counts significantly correlated with levels of CXCL10 and CXCL9 but not with those of CCL5 or CCL4, the negative control (Fig. 1A). In addition, the correlation was clearly stronger with CXCL10 than with CXCL9. Following this, we compared the CSF and serum levels of these chemokines. Interestingly, only CXCL10 levels were higher in the CSF than the serum, although serum CXCL10 levels were also high to some extent (Fig. 1B, $P < 0.0001$). Next, to investigate whether these high CXCL10 levels were a HAM/TSP-specific phenomenon within HTLV-1-associated disorders, we tested for a correlation between CXCL10 and soluble interleukin-2 receptor (sIL-2R), a marker for adult T cell leukaemia (Yasuda et al., 1988). As expected, serum sIL-2R levels were the highest in patients with adult T cell leukaemia. By contrast, plasma CXCL10 levels were significantly higher in patients with HAM/TSP than in those with adult T cell leukaemia, asymptomatic carriers or healthy donors (Supplementary Fig. 1A). This higher concentration of plasma CXCL10 in patients with HAM/TSP was observed even when compared to asymptomatic carriers with equivalently high proviral loads (Supplementary Fig. 1B).

Existence of abundant $CXCR3^+$ cells in the spinal cords of patients with HAM/TSP

Because CXCL10 is a ligand of CXCR3, we investigated the possibility of CXCL10 recruiting proinflammatory $CXCR3^+$ cells into the CSF by measuring the presence of $CXCR3^+$ cells in the CSF and spinal cord lesions of patients with HAM/TSP (Fig. 2A–C). Flow cytometric analysis revealed that the average percentage of

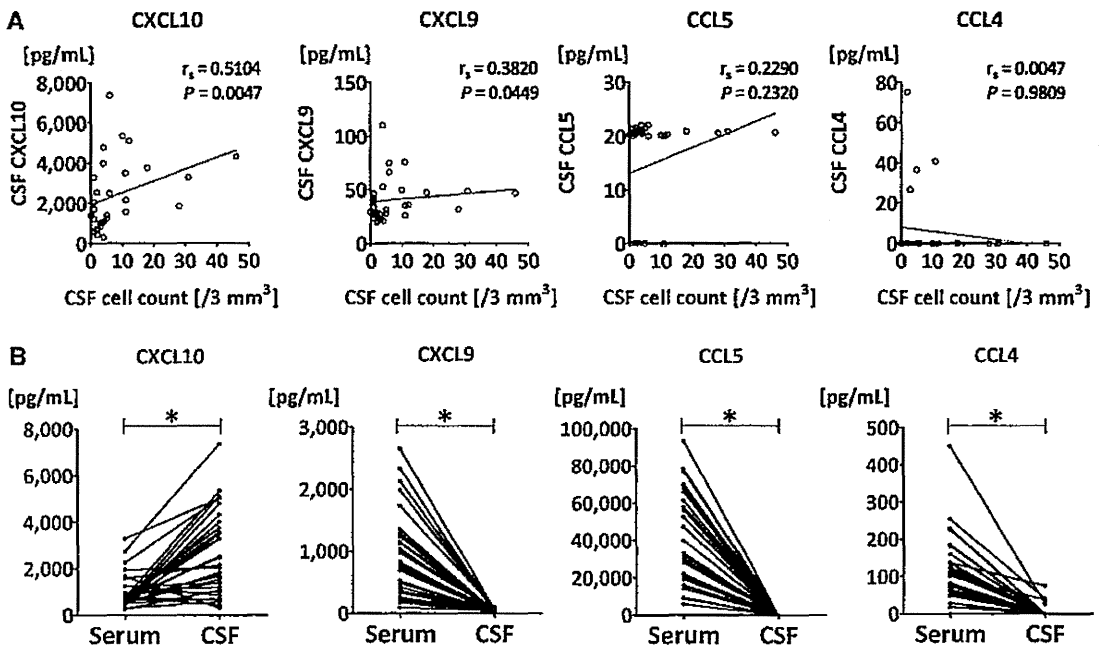

Figure 1 CXCL10 levels in CSF of patients with HAM/TSP were correlated with CSF cell counts and were significantly higher than those in serum of patients with HAM/TSP. (A) Correlation analysis between CSF levels of four chemokines (CXCL10, CXCL9, CCL5 and CCL4) and CSF cell counts in patients with HAM/TSP ($n = 29$). Statistical analysis was performed using Spearman's rank test. The linear regression line is indicated by a straight line in each graph. (B) Comparison of concentrations of four chemokines (CXCL10, CXCL9, CCL5, and CCL4) in CSF and serum samples obtained from patients with HAM/TSP such that all samples from a given patient were taken within a 1-h window of the first sample taken from that patient ($n = 32$). *$P < 0.0001$ by the paired t-test.

CXCR3$^+$ cells among CSF cells was 92.4 ± 7.0%, whereas the average percentage of CXCR3$^+$ cells among peripheral blood mononuclear cells was 9.9 ± 8.2% ($P < 0.0001$, Fig. 2B). Immunofluorescence staining revealed abundant CXCR3$^+$ cell infiltrate around small vessels in the leptomeninges of spinal cord lesions in patients with HAM/TSP (Fig. 2C). We examined the types of CXCR3$^+$ cells in the CSF using flow cytometry and found that CSF CXCR3$^+$ cells mainly consist of CD3$^+$ cells (>90%) and small populations of CD14$^+$ and CD19$^+$ cells (Fig. 2D, left). Uniquely, the percentage of CXCR3$^+$ cells was extremely high in all CSF cell populations under study, especially CD4$^+$ (94.33 ± 2.95%), CD8$^+$ (98.64 ± 1.05%), and even CD14$^+$ (84.97 ± 18.49%) and CD19$^+$ (76.38 ± 17.35%) cells (Supplementary Fig. 2). Our data show that the ratio of CD4$^+$ to CD8$^+$ cells in the CSF was ~1:1 in patients with HAM/TSP (Fig. 2D, right). In both these cell populations, the rate of CXCR3 positivity was higher in CSF cells than in peripheral blood mononuclear cells (Supplementary Fig. 2). The percentage of CXCR3$^+$ cells in peripheral blood mononuclear cells of patients with HAM/TSP was lower than those in peripheral blood mononuclear cells of asymptomatic carriers as well as healthy donors; however, there were no significant differences between patients with adult T cell leukaemia and patients with HAM/TSP (Supplementary Fig. 3A). This lower percentage of CXCR3$^+$ cells in patients with HAM/TSP was observed even when compared with asymptomatic carriers with equivalently high proviral loads (Supplementary Fig. 3B). Finally, to support our hypothesis that HTLV-1-infected T cells (the majority of which are known to be CD4$^+$) migrate from the circulating blood to the spinal cord tissue through CXCL10–CXCR3 interaction, we confirmed that there does exist a subset of peripheral CD4$^+$CXCR3$^+$ T cells infected with HTLV-1 (Fig. 2E).

Numerous CXCL10-producing cells in inflamed spinal cords of patients with HAM/TSP

To quantitatively compare the level of expression of CXCL10, we microscopically counted the number of CXCL10$^+$ cells in the spinal cord tissue and found a larger number of CXCL10$^+$ cells in the spinal cord lesions of patients with HAM/TSP than in control patients (Fig. 3A, $P = 0.0095$). In addition, we compared tissue sections from the thoracic spinal cord (a region of high inflammation) and the medulla oblongata (comparatively very low inflammation) from a single patient with HAM/TSP, and we observed a much larger CXCL10 presence in the thoracic spinal cord region (Supplementary Fig. 4).

Astrocytes as the main producers of CXCL10 in the spinal cords of patients with HAM/TSP

To identify which cell populations are the main CXCL10 producers, we immunostained thoracic spinal cord tissues from patients with

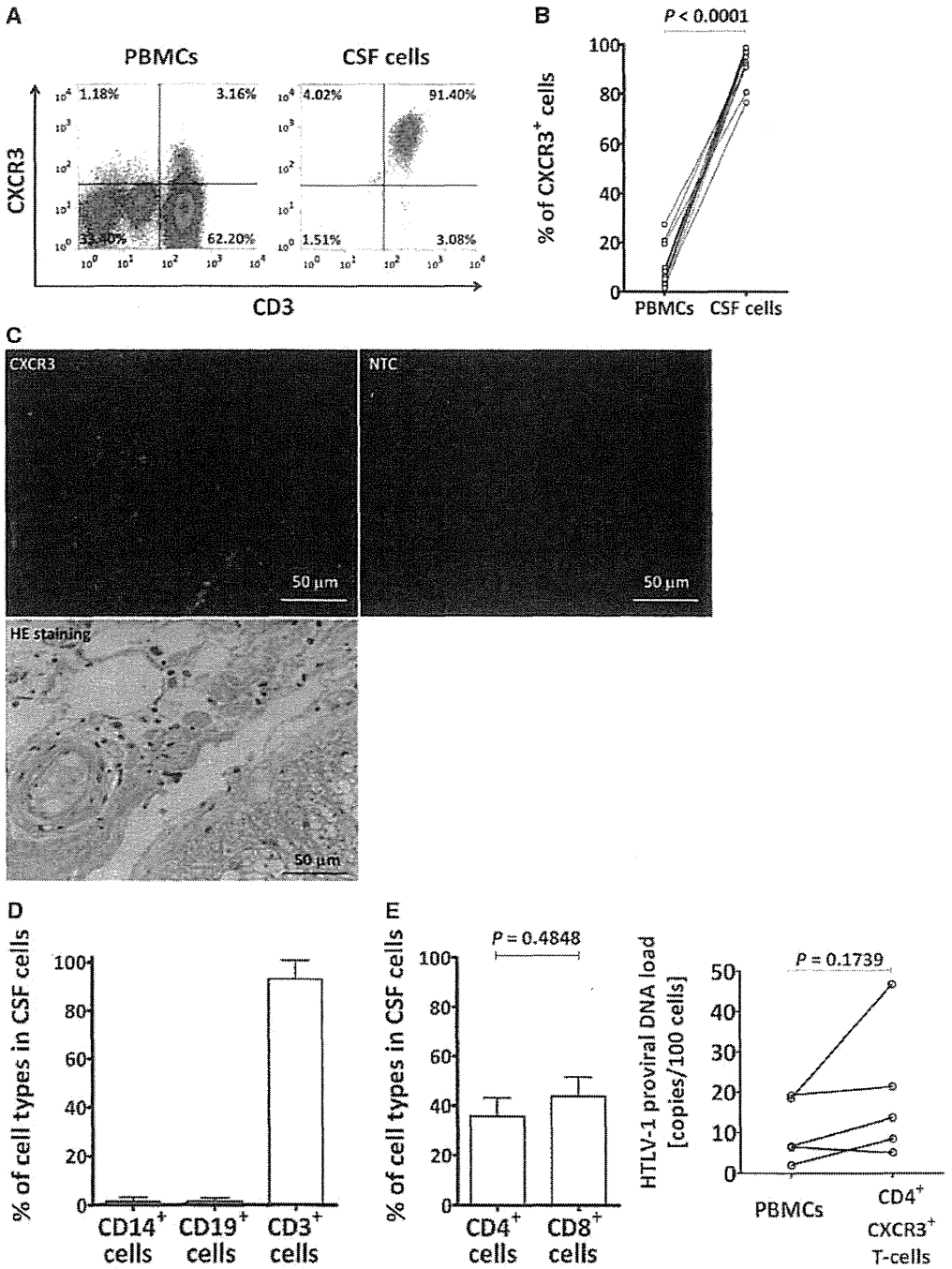

Figure 2 Abundant CXCR3$^+$ cells in the CSF and spinal cord tissue of patients with HAM/TSP. (**A**) Representative dot plots of CD3 and CXCR3 expression in peripheral blood mononuclear cells (PBMCs, *left*) and CSF cells (*right*) from a patient with HAM/TSP measured using flow cytometry. (**B**) Comparison of the percentages of CXCR3$^+$ cells in peripheral blood mononuclear cells and CSF cells, samples of which were obtained from 12 patients with HAM/TSP such that all samples from a given patient were taken within a 1-h window of the first sample taken from that patient. Statistical analysis was performed using the paired *t*-test. See also Supplementary Fig. 2. (**C**) Representative images of immunofluorescent detection of CXCR3, shown in green (*upper* panels), and haematoxylin-eosin (HE) staining for inflammatory cells, shown in blue (*lower* panel), in the thoracic spinal cords of patients with HAM/TSP. Rabbit IgG antibody used as the negative control (NTC). (**D**) *Left*: Percentages of CD3$^+$, CD19$^+$, and CD14$^+$ cells in CSF cells derived from patients with HAM/TSP ($n = 6$). *Right*: Percentages of CD4$^+$ cells and CD8$^+$ cells. Statistical analysis was performed using the Mann–Whitney U-test. Error bars represent the mean ± SD. (**E**) The HTLV-1 proviral DNA loads of CD4$^+$CXCR3$^+$ T cells with peripheral blood mononuclear cells as the control. This result confirms the non-negligible existence of HTLV-1-infected CD4$^+$CXCR3$^+$ T cells, which may migrate to the CNS. Cells are from patients with HAM/TSP ($n = 5$). Statistical analysis was performed using the paired *t*-test.

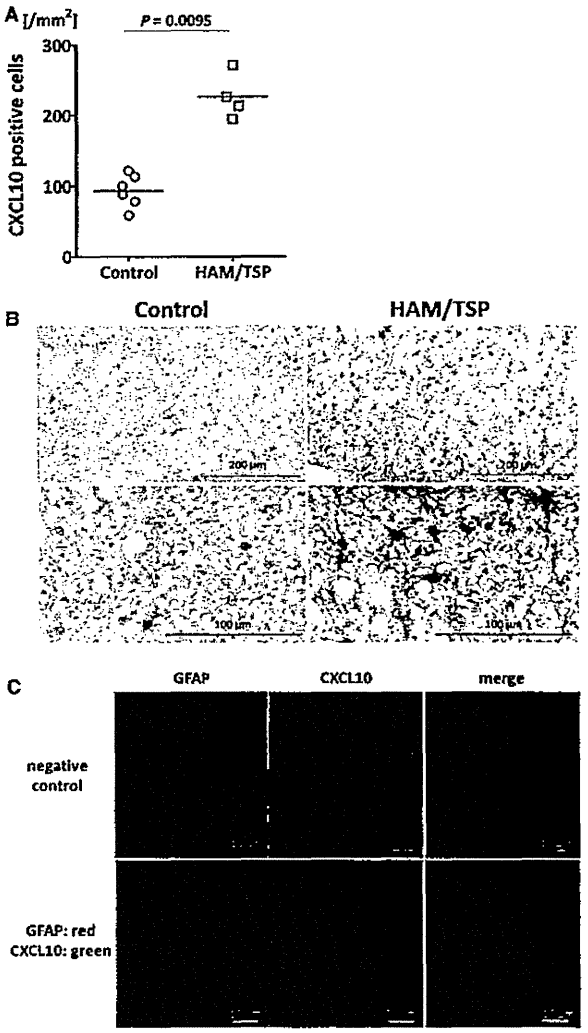

Figure 3 Astrocytes are the major CXCL10-producing cells in the spinal cords of patients with HAM/TSP. (**A**) Quantitative histological analysis (control: $n = 6$, HAM/TSP: $n = 4$). The numbers of CXCL10$^+$ cells in the spinal cord sections were counted under a microscope. The data represent the mean number of CXCL10$^+$ cells in three random fields of 1 mm^2 per sample. Horizontal bars represent the mean. Statistical analysis was performed using the Mann–Whitney U-test. (**B**) Representative immunohistochemistical images of CXCL10 in the thoracic spinal cord tissues from control individuals ($n = 6$) and patients with HAM/TSP ($n = 4$). CXCL10-positive cells are brown. *Upper* panel: low magnification; *Lower* panel: high magnification. (**C**) Representative immunofluorescent images of GFAP (red), a marker for astrocytes, and CXCL10 (green) in the thoracic spinal cord tissues from a control individual and a patient with HAM/TSP patient. Similar results were observed in images of spinal cord tissues obtained from two other patients with HAM/TSP.

HAM/TSP ($n = 4$) and control individuals ($n = 6$). CXCL10-positive staining was mainly observed in star-shaped cells with extensive and radiating cytoplasmic processes, indicating that CXCL10 is expressed in activated astrocytes in the thoracic spinal cord of patients with HAM/TSP (Fig. 3B). We also used immunofluorescence to confirm that CXCL10 is mainly expressed in astrocytes (GFAP$^+$ cells) (Fig. 3C).

Co-culture with CD4$^+$ T cells from patients with HAM/TSP enhances CXCL10 production in U251 human astrocytoma cells

CXCL10, also known as an IFN-γ-inducible protein 10, is mainly produced in response to IFN-γ stimulation (Muller *et al.*, 2010). We used this fact to investigate the events leading to CXCL10 production by astrocytes in the spinal cords of patients with HAM/TSP. First, we compared the capacities of several purified cell populations within peripheral blood mononuclear cells to produce IFN-γ spontaneously, i.e. without any stimulation. We found that CD4$^+$ T cells exhibited the highest production of IFN-γ among peripheral blood mononuclear cells isolated from patients with HAM/TSP, and CD4$^+$ T cells from patients with HAM/TSP produced more IFN-γ than those from asymptomatic carriers (Fig. 4A and B left). No peripheral blood mononuclear cells isolated from healthy donors displayed any detectable level of IFN-γ production (data not shown). Interestingly, CD4$^+$ T cells from patients with HAM/TSP did not produce IL-17A, a proinflammatory cytokine known to play a key role in the pathogenic inflammatory response that characterizes multiple sclerosis (Fig. 4B, right) (Matusevicius *et al.*, 1999). Next, we used a co-culture system to confirm that CD4$^+$ T cells induce astrocytes to produce CXCL10 by releasing IFN-γ. CD4$^+$ T cells from patients with HAM/TSP induced CXCL10 production in U251 astrocytoma cells in a cell number-dependent manner (Fig. 4C), whereas CD4$^+$ T cells from healthy donors did not induce CXCL10 production (data not shown). Importantly, in the presence of anti-IFN-γ neutralizing antibodies, the supernatant from HAM/TSP patient CD4$^+$ T cell cultures stimulated significantly less CXCL10 production in U251 cells (Fig. 4D).

Chemotaxis of peripheral blood mononuclear cells from patients with HAM/TSP due to CXCL10 and inhibition of chemotaxis by anti-CXCL10 neutralizing antibodies

To investigate the potential role of CXCL10 or CXCR3 as a therapeutic target for inhibiting the migration of proinflammatory cells into the CNS, we assessed whether neutralizing antibodies against CXCL10 or CXCR3 could inhibit the migration of peripheral blood mononuclear cells in patients with HAM/TSP through the use of an *in vitro* chemotaxis assay system. Human CXCL10 increased the chemotactic activity of peripheral blood mononuclear cells from patients with HAM/TSP by ~1.7-fold (Fig. 5A). Compared with isotype control monoclonal antibodies, the chemotactic activity due to CXCL10 was inhibited by anti-CXCL10 neutralizing antibodies (Fig. 5A; 65.9% inhibition, $P < 0.01$) but not by anti-CXCR3 antibodies (Fig. 5A; 9.2% inhibition, $P > 0.05$: not

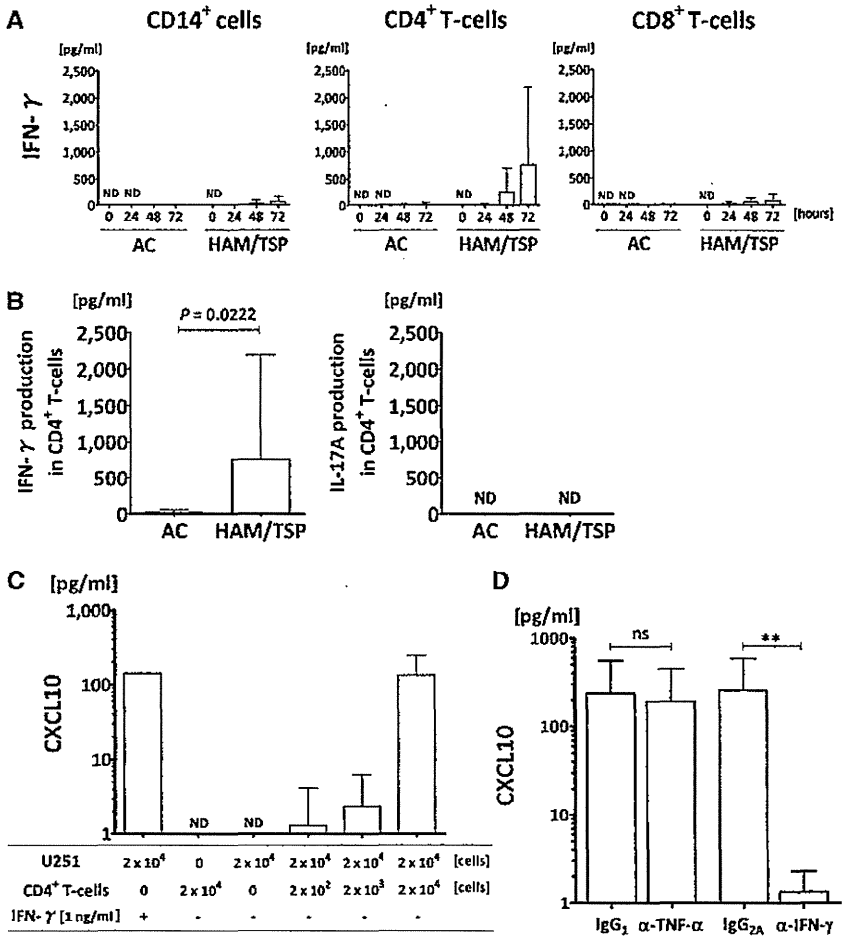

Figure 4 Co-culturing with CD4+ T cells from patients with HAM/TSP increases CXCL10 production in a U251 human astrocytoma cell line. (A) Concentration of IFN-γ in supernatants of cultured CD4+, CD8+, or CD14+ cells in peripheral blood mononuclear cells (PBMCs) from patients with HAM/TSP ($n = 6$) compared with that in peripheral blood mononuclear cells from asymptomatic carriers (AC, $n = 5$). These cells were cultured without any stimuli for 24, 48 and 72 h. ND = not detected. (B) Concentrations of IFN-γ (*left*) and IL-17A (*right*) in culture supernatants of cultured CD4+ T cells for 72 h from patients with HAM/TSP compared with the concentrations in those from asymptomatic carriers. Patients with HAM/TSP: $n = 6$, asymptomatic carrier: $n = 5$. ND = not detected. Statistical analyses were performed using the Mann–Whitney U-test. (C) Concentration of CXCL10 produced by U251, a human astrocytoma cell line, co-cultured with CD4+ T cells from patients with HAM/TSP ($n = 5$). ND = not detected. (D) Concentration of CXCL10 produced by U251 stimulated by the supernatant of cultured CD4+ T cells of patients with HAM/TSP ($n = 5$) in the presence of neutralizing antibodies against IFN-γ and TNF-α, and isotype control antibodies for each. NS = not significant. $^{**}P < 0.01$. Error bars represent the mean ± SD.

significant). Next, we investigated whether or not this decreased migration would also be reflected in the absolute number of HTLV-1-infected cells among migrated cells. Chemotaxis assays revealed that the addition of human CXCL10 (0.25 μg/ml) increased the absolute number of HTLV-1-infected cells by ~2.1-fold (Fig. 5B) compared with isotype control monoclonal antibodies, and that this increase was largely inhibited by anti-CXCL10 neutralizing antibodies (Fig. 5B; 101.1% inhibition, $P < 0.01$) but only slightly by anti-CXCR3 antibodies (Fig. 5B; 65.7% inhibition, $P > 0.05$: not significant). Finally, we evaluated the degree to which the migrated cells were proliferating spontaneously, where spontaneous proliferation is defined as proliferation in the absence of exogenous antigens or stimulants (Itoyama *et al.*, 1988; Ijichi *et al.*, 1989). This is important because the level of spontaneous proliferation of peripheral blood mononuclear cells in patients with HAM/TSP is believed to reflect the cell proliferation that occurs in the CNS (Itoyama *et al.*, 1988; Ijichi *et al.*, 1989). Significantly less ^{3}H-thymidine uptake, an assay for cell proliferation, was detected in the lower chemotaxis assay chamber following administration of anti-CXCL10 antibody than isotype control antibodies (Fig. 5C; 33.8% inhibition, $P < 0.05$).

Discussion

Previous studies of HAM/TSP pathogenesis have revealed that chronic inflammation occurs in the spinal cords of patients with HAM/TSP (Saito and Bangham, 2012; Yamano and Sato, 2012);

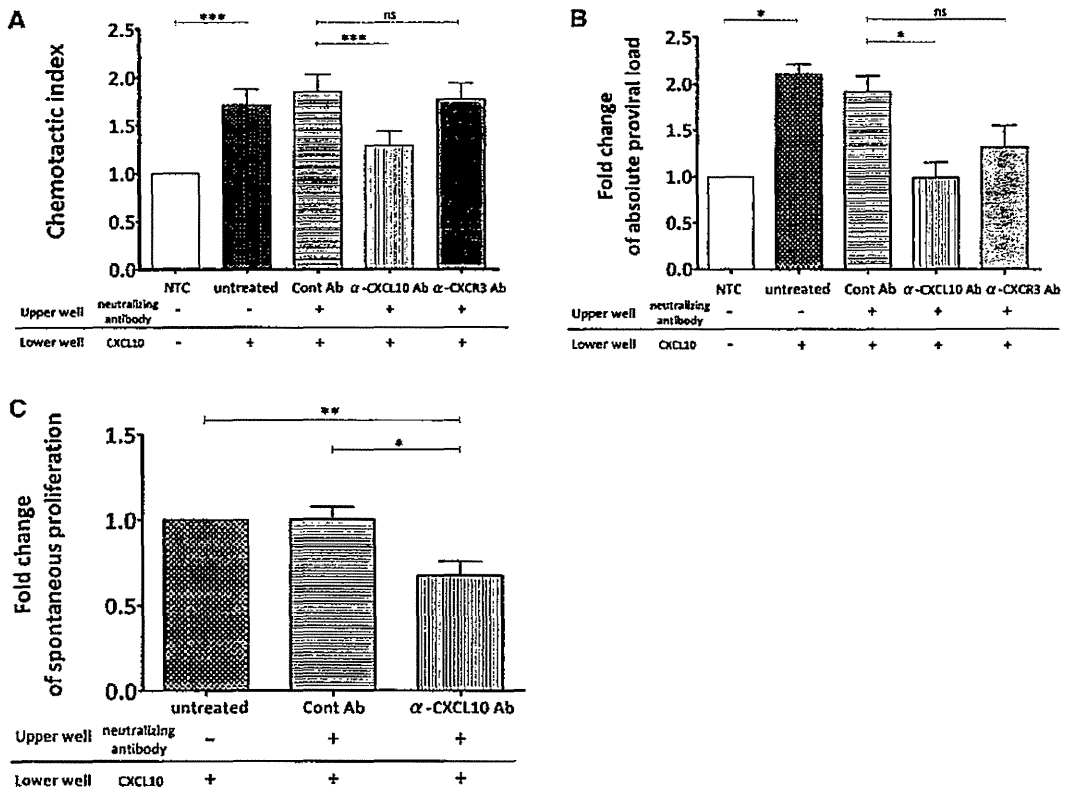

Figure 5 Chemotaxis of peripheral blood mononuclear cells due to CXCL10 and inhibition of chemotaxis by anti-CXCL10 neutralizing antibody in cells from patients with HAM/TSP. (**A**) The migration-inducing effect of CXCL10 and the inhibitory effect of neutralizing antibody against CXCL10 versus its receptor, CXCR3. Peripheral blood mononuclear cells from patients with HAM/TSP ($n = 21$) migrated into the lower well in response to CXCL10, and treatment with anti-CXCL10 antibody significantly reduced the migration of peripheral blood mononuclear cells, as compared to anti-CXCR3 antibody and control antibody. (**B**) The inhibition of cell migration led to an overall decrease in migrated cells including HTLV-1-infected cells, effectively decreasing the absolute proviral load. Peripheral blood mononuclear cells used were collected from patients with HAM/TSP; $n = 4$. (**C**) The inhibition of cell migration led to an overall decrease in migrated cells which also means less spontaneous proliferation. Peripheral blood mononuclear cells used were collected from patients with HAM/TSP; $n = 7$. Error bars represent the mean ± SD. Statistical analyses were performed using the Friedman test followed by the Dunn test for multiple comparison. NS = not significant. $^*P < 0.05$, $^{**}P < 0.01$, $^{***}P < 0.001$. NTC = negative control; Cont Ab = isotype control monoclonal antibody; α-CXCL10 Ab = anti-CXCL10 monoclonal antibody; α-CXCR3 Ab = anti-CXCR3 monoclonal antibody.

however, the precise mechanisms by which these inflammatory lesions are formed and maintained remain unclear. We hypothesized that a positive feedback loop driven by chemokines may be responsible for the chronic inflammation associated with HAM/TSP. We identified CXCL10 as the principal chemokine responsible for inducing this chronic inflammation. We found for the first time astrocytes to be the main producers of CXCL10. Our data suggest that these astrocytes are stimulated to produce CXCL10 initially by IFN-γ released by infected T cells, where the infection appears to have produced changes in the cells that promote spontaneous IFN-γ production. In short, we inferred that spinal cord lesions found in patients with HAM/TSP arise when IFN-γ produced by HTLV-1-infected T cells induces astrocytes to secrete CXCL10, which attracts $CXCR3^+$ T cells, including more T cells infected with HTLV-1, thereby continuing the cycle. Furthermore, we demonstrated that an interruption of this pathway represents a promising strategy for treating HAM/TSP.

First, we identified the key chemokine involved in inducing the migration of cells to sites of inflammation. We compared the CSF and serum levels of several chemokines and demonstrated for the first time that CXCL10 is the only chemokine of those studied that is present at a significantly higher concentration in the CSF than in the sera of patients with HAM/TSP. Although previous reports indicate that CCL5 and CXCL9 levels are also elevated in the CSF of patients with HAM/TSP (Teixeira *et al.*, 2004; Tanaka *et al.*, 2008), we showed that these two chemokines exhibit a concentration gradient in the opposite direction (Fig. 1B). We previously measured the levels of other chemokines such as CCL3, CCL4, CXCL11, CCL17, CCL20 and CCL22 in the CSF and found that the levels of these chemokines are negligible in patients with HAM/TSP (Sato, in press). Importantly, we also previously demonstrated that CSF CXCL10 levels are correlated with the rate of disease progression (Sato, in press). These findings suggest that CXCL10 is crucial for the development of chronic inflammation in patients with HAM/TSP.

In the present study, we found a positive correlation between CSF CXCL10 levels and CSF cell counts (Fig. 1A), a high percentage of CXCR3-positive cells in the CSF (Fig. 2A and B; 92.4 ± 7.0%), and perivascular accumulation of $CXCR3^+$ cells in spinal cord lesions of patients with HAM/TSP (Fig. 2C). These results strongly indicate that a high concentration of CXCL10 in the spinal cord attracts $CXCR3^+$ cells that include proinflammatory cells (Qin *et al.*, 1998; Sallusto *et al.*, 1998; Thomas *et al.*, 2003). Intriguingly, the percentage of $CXCR3^+$ cells among peripheral blood mononuclear cells from patients with HAM/TSP was significantly lower than that observed in asymptomatic carriers and healthy donors, but not patients with adult T cell leukaemia (Supplementary Fig. 3). $CXCR3^+$ peripheral blood mononuclear cells are relatively few in patients with adult T cell leukaemia, perhaps because of an increase in $CCR4^+CXCR3^-$ tumour cells in the peripheral blood (Ishida *et al.*, 2003). Although the precise mechanism by which peripheral $CXCR3^+$ cells in patients with HAM/TSP become diminished remains unclear, we believe that many of these cells migrate into the CNS and contribute to the formation of spinal cord lesions. Other possible mechanisms include migration to lymphoid organs such as lymph nodes or the spleen. Because lymph nodes are important organs for CXCL10–CXCR3 interactions in patients suffering from various diseases (Groom *et al.*, 2012; Sung *et al.*, 2012), future studies analysing the lymph nodes of patients with HAM/TSP may provide a more complete understanding of HAM/TSP pathogenesis.

The discovery that CXCL10–CXCR3 interactions represent an important pathway for recruiting cells to the CNS in patients with HAM/TSP prompted us to search the spinal cord lesions of patients with HAM/TSP and identify the CXCL10-producing cells. Firstly, we confirmed that CXCL10-producing cells are more numerous in the spinal cords of patients with HAM/TSP than control individuals (Fig. 3A). We also compared high and low inflammatory regions within a single patient with HAM/TSP and found more CXCL10-producing cells in the more inflamed region (Supplementary Fig. 4), although the limitation of sampling from only a single individual prevents us from extrapolating too freely on the significance of this result. Although CXCL10 is secreted by several cell types such as monocytes, endothelial cells, fibroblasts and astrocytes in response to IFN-γ (Luster and Ravetch, 1987; Lee *et al.*, 2009), our study demonstrated that astrocytes are the major CXCL10-producing cells in thoracic spinal cord lesions in patients with HAM/TSP (Fig. 3). Notably, the astrocytes examined in this study were star-shaped with radiating cytoplasmic processes, indicating high cytological activity (Fig. 3B and C). In the CNS, CXCL10 is mainly produced by astrocytes; however, CXCL9 is primarily a product of microglial cells (Muller *et al.*, 2010). Therefore, the finding that CXCL10 production is substantially higher than CXCL9 production in the CSF (Fig. 1) suggests that astrocytes are very active in HAM/TSP. This finding supports a previous finding that gliosis is one of the main pathological features of HAM/TSP (Iwasaki, 1990; Izumo *et al.*, 1992).

Next, we investigated the mechanism by which astrocytes produce CXCL10 in patients with HAM/TSP. CXCL10 is generally not detectable in most non-lymphoid tissues under physiological conditions; however, its synthesis is easily induced by cytokines, particularly IFN-γ. Therefore, it was important to determine the source of IFN-γ that stimulates astrocytes to produce CXCL10 in patients with HAM/TSP. Interestingly, we have shown that $CD4^+$ T cells from patients with HAM/TSP spontaneously produce IFN-γ and induce CXCL10 production by U251 human astrocytoma cells via IFN-γ (Fig. 4), whereas $CD4^+$ T cells from healthy donors do not induce CXCL10 production (data not shown). These results support the hypothesis that there are interactions between HTLV-1-infected $CD4^+$ T cells and astrocytes in patients with HAM/TSP *in vivo* that may possibly initiate the first wave of CXCL10 production. Moreover, this CXCL10 production may further induce the trafficking of peripheral $CXCR3^+$ T cells. Importantly, we demonstrated that a number of peripheral $CXCR3^+$ T cells are infected with HTLV-1 (Fig. 2E), indicating that migration of peripheral $CXCR3^+$ T cells into the CNS can induce further secretion of IFN-γ that continues the vicious cycle. In fact, HTLV-1-infected $CD4^+$ T cells and IFN-γ-producing T cells have been detected in HAM/TSP spinal cord lesions (Umehara *et al.*, 1994; Moritoyo *et al.*, 1996; Matsuoka *et al.*, 1998). Notably, more than half of the $CXCR3^+$ T cells in the CSF of patients with HAM/TSP are $CD8^+$ T cells (Fig. 2D). It has been shown that $CD8^+$ cytotoxic T lymphocytes (CTLs), particularly HTLV-1-specific CTLs, have a high potential for secreting IFN-γ (Kubota *et al.*, 2000; Hanon *et al.*, 2001) and are abnormally elevated in the CSF and spinal cord lesions (Nagai *et al.*, 2001*a*, *b*; Matsuura *et al.*, 2010). Therefore, CXCL10 production by astrocytes may further boost the trafficking of $CXCR3^+$-infected $CD4^+$ T cells as well as $CXCR3^+CD8^+$ CTLs that secrete IFN-γ, leading to a positive feedback-driven chronic inflammatory loop.

The results of the present study and other studies show that the pathology of HAM/TSP is unique among immune disorders. Unlike other inflammatory disorders such as multiple sclerosis or rheumatoid arthritis that exhibit Th17 as well as Th1 involvement (Matusevicius *et al.*, 1999; Kirkham *et al.*, 2006), HAM/TSP pathogenesis appears to be dominated by the Th1 axis, particularly CXCL10–CXCR3 interactions. Our research indicates that the characteristics of HTLV-1-infected T cells may be responsible for the emphasis on the Th1 axis in HAM/TSP pathogenesis. We have reported that cultured $CD4^+$ T cells from patients with HAM/TSP clearly exhibit detectable production of IFN-γ (a Th1 cytokine) but not IL-17 (a Th17 cytokine) (Fig. 4B), and we previously demonstrated that HTLV-1-infected T cells in patients with HAM/TSP exhibit elevated IFN-γ and reduced IL-17 production (Yamano *et al.*, 2009). Furthermore, HAM/TSP peripheral blood contained more CXCL10 (Supplementary Fig. 1B) and fewer $CXCR3^+$ cells (Supplementary Fig. 3B) than asymptomatic carrier blood, suggesting that a greater number of $CXCR3^+$ cells had migrated out of the periphery due at least in part to chemotaxis induced by elevated CXCL10 production in the CNS. As the proviral loads of all the samples used in the above experiment were roughly identically high, it can be assumed that these characteristics are indeed features of HAM/TSP pathogenesis as opposed to simple consequences of having a high proviral load.

We suspect that a genetic predisposition for higher IFN-γ or CXCL10 production in response to HTLV-1 may exist. Recently, systems biology approaches were used to show that a subset of IFN-stimulated genes, including the gene encoding CXCL10, is overexpressed in peripheral blood mononuclear cells of patients with HAM/TSP compared with asymptomatic carriers

(Tattermusch *et al.*, 2012). It will be important to test for an association between genetic polymorphisms in interferon-associated genes and the presence of HAM/TSP in future studies. The existence of this genetic predisposition would strengthen the argument for Th1-dominance and explain why some infected individuals develop HAM/TSP, whereas others remain life-long asymptomatic carriers. Because it is well-known that interferons and products of interferon-stimulated genes mediate antiviral responses (Randall and Goodbourn, 2008), IFN-γ and CXCL10 production in HTLV-1-infected patients (Supplementary Fig. 1) may be considered a normal immune response. However, once the production levels surpass threshold and a CXCL10–CXCR3 amplification loop develops, it may begin to cause tissue damage. Possible reasons for CXCL10 overproduction in HAM/TSP include the presence of a high number of HTLV-1-infected T cells (Nagai *et al.*, 1998; Yamano *et al.*, 2002) and a genetic predisposition for higher IFN-γ and/or CXCL10 production in response to HTLV-1.

The ideal therapeutic strategy for treating HAM/TSP would be eradication of HTLV-1-infected cells, but this has yet to be proven possible. Another promising approach would be a receptor blockade using anti-CXCR3 neutralizing antibody, which has been reported to be effective at blocking CXCR3 activity (Van den Steen *et al.*, 2008). Although we were unable to validate this effect using our commercially available antibody, this certainly does not rule out a receptor blockade as a therapeutic candidate. Our relative success at disrupting inflammatory cell migration using anti-CXCL10 neutralizing antibodies (Fig. 5) suggests that targeting CXCL10 to interrupt the positive feedback loop may be the more promising new strategy for effectively treating HAM/TSP. A noteworthy potential advantage of anti-CXCL10 over anti-CXCR3 is that it may yield less severe side effects as only interactions with CXCL10 rather than all CXCR3 agonists would be blocked.

In conclusion, our data revealed novel insights into the pathogenic processes of HAM/TSP. Our results suggest that CXCL10 plays a pivotal role in the development of chronic inflammatory lesions where HTLV-1-infected T cells produce IFN-γ, which induces astrocytes to secrete CXCL10. This further boosts the trafficking of $CXCR3^+$-infected T cells that secrete IFN-γ, leading to a virus-induced CXCL10–CXCR3 inflammatory loop. Thus, HAM/TSP represents a pathological consequence of interactions that occur between the immune system and CNS. Understanding these complex interactions should provide new insights into the functional regulation of both systems and help uncover new therapeutic targets.

Acknowledgements

The authors thank K. Takahashi, Y. Kunitomo, Y. Sato, Y. Suzuki, M. Koike, and Y. Hasegawa for technical assistance.

Funding

This work was partly supported by project "Research on Measures for Intractable Disease," a matching fund subsidy from the Ministry of Health Labour and Welfare, a Grant-in-Aid for Scientific Research from the Ministry of Education, Culture, Sports, Science and Technology, and the MEXT-Supported Program for the Strategic Research Foundation at Private Universities, 2008–2012.

Supplementary material

Supplementary material is available at *Brain* online.

References

Furuya T, Nakamura T, Shirabe S, Nishiura Y, Tsujino A, Goto H, et al. Heightened transmigrating activity of CD4-positive T cells through reconstituted basement membrane in patients with human T-lymphotropic virus type I-associated myelopathy. Proc Assoc Am Physicians 1997; 109: 228–36.

Gessain A, Barin F, Vernant JC, Gout O, Maurs L, Calender A, et al. Antibodies to human T-lymphotropic virus type-I in patients with tropical spastic paraparesis. Lancet 1985; 2: 407–10.

Goon PK, Hanon E, Igakura T, Tanaka Y, Weber JN, Taylor GP, et al. High frequencies of Th1-type CD4(+) T cells specific to HTLV-1 env and tax proteins in patients with HTLV-1-associated myelopathy/tropical spastic paraparesis. Blood 2002; 99: 3335–41.

Groom JR, Richmond J, Murooka TT, Sorensen EW, Sung JH, Bankert K, et al. CXCR3 chemokine receptor-ligand interactions in the lymph node optimize CD4(+) T helper 1 cell differentiation. Immunity 2012; 37: 1091–103.

Hanon E, Goon P, Taylor GP, Hasegawa H, Tanaka Y, Weber JN, et al. High production of interferon gamma but not interleukin-2 by human T-lymphotropic virus type I-infected peripheral blood mononuclear cells. Blood 2001; 98: 721–6.

Hinuma Y, Nagata K, Hanaoka M, Nakai M, Matsumoto T, Kinoshita KI, et al. Adult T-cell leukemia: antigen in an ATL cell line and detection of antibodies to the antigen in human sera. Proc Natl Acad Sci USA 1981; 78: 6476–80.

Ijichi S, Eiraku N, Osame M, Izumo S, Kubota R, Maruyama I, et al. In vitro modulation of lymphocyte proliferation by prednisolone and interferon-alpha in patients with HTLV-I-associated myelopathy (HAM). J Neuroimmunol 1989; 23: 175–8.

Ishida T, Utsunomiya A, Iida S, Inagaki H, Takatsuka Y, Kusumoto S, et al. Clinical significance of CCR4 expression in adult T-cell leukemia/lymphoma: its close association with skin involvement and unfavorable outcome. Clin Cancer Res 2003; 9: 3625–34.

Itoyama Y, Minato S, Kira J, Goto I, Sato H, Okochi K, et al. Spontaneous proliferation of peripheral blood lymphocytes increased in patients with HTLV-I-associated myelopathy. Neurology 1988; 38: 1302–7.

Iwasaki Y. Pathology of chronic myelopathy associated with HTLV-I infection (HAM/TSP). J Neurol Sci 1990; 96: 103–23.

Izumo S, Ijichi T, Higuchi I, Tashiro A, Takahashi K, Osame M. Neuropathology of HTLV-I-associated myelopathy—a report of two autopsy cases. Acta Paediatr Jpn 1992; 34: 358–64.

Jacobson S, Shida H, McFarlin DE, Fauci AS, Koenig S. Circulating CD8(plus) cytotoxic T lymphocytes specific for HTLV-I pX in patients with HTLV-I associated neurological disease. Nature 1990; 348: 245–8.

Jeffery KJ, Usuku K, Hall SE, Matsumoto W, Taylor GP, Procter J, et al. HLA alleles determine human T-lymphotropic virus-I (HTLV-I) proviral load and the risk of HTLV-I-associated myelopathy. Proc Natl Acad Sci USA 1999; 96: 3848–53.

Kirkham BW, Lassere MN, Edmonds JP, Juhasz KM, Bird PA, Lee CS, et al. Synovial membrane cytokine expression is predictive of joint damage progression in rheumatoid arthritis: a two-year prospective study (the DAMAGE study cohort). Arthritis Rheum 2006; 54: 1122–31.

Kubota R, Kawanishi T, Matsubara H, Manns A, Jacobson S. HTLV-I specific IFN-gamma+ CD8+ lymphocytes correlate with the proviral load in peripheral blood of infected individuals. J Neuroimmunol 2000; 102: 208–15.

Lee EY, Lee ZH, Song YW. CXCL10 and autoimmune diseases. Autoimmun Rev 2009; 8: 379–83.

Libby P. Inflammation in atherosclerosis. Nature 2002; 420: 868–74.

Luster AD. Chemokines—chemotactic cytokines that mediate inflammation. N Engl J Med 1998; 338: 436–45.

Luster AD, Ravetch JV. Biochemical characterization of a gamma interferon-inducible cytokine (IP-10). J Exp Med 1987; 166: 1084–97.

Mantovani A, Allavena P, Sica A, Balkwill F. Cancer-related inflammation. Nature 2008; 454: 436–44.

Matsuoka E, Takenouchi N, Hashimoto K, Kashio N, Moritoyo T, Higuchi I, et al. Perivascular T cells are infected with HTLV-I in the spinal cord lesions with HTLV-I-associated myelopathy/tropical spastic paraparesis: double staining of immunohistochemistry and polymerase chain reaction in situ hybridization. Acta Neuropathol 1998; 96: 340–6.

Matsuura E, Yamano Y, Jacobson S. Neuroimmunity of HTLV-I infection. J Neuroimmune Pharmacol 2010; 5: 310–25.

Matusevicius D, Kivisakk P, He B, Kostulas N, Ozenci V, Fredrikson S, et al. Interleukin-17 mRNA expression in blood and CSF mononuclear cells is augmented in multiple sclerosis. Mult Scler 1999; 5: 101–4.

Medzhitov R. Inflammation 2010: new adventures of an old flame. Cell 2010; 140: 771–6.

Medzhitov R. Origin and physiological roles of inflammation. Nature 2008; 454: 428–35.

Moritoyo H, Arimura K, Arimura Y, Tokimura Y, Rosales R, Osame M. Study of lower limb somatosensory evoked potentials in 96 cases of HTLV-I-associated myelopathy/tropical spastic paraparesis. J Neurol Sci 1996; 138: 78–81.

Muller M, Carter S, Hofer MJ, Campbell IL. Review: the chemokine receptor CXCR3 and its ligands CXCL9, CXCL10 and CXCL11 in neuroimmunity—a tale of conflict and conundrum. Neuropathol Appl Neurobiol 2010; 36: 368–87.

Nagai M, Yamano Y, Brennan MB, Mora CA, Jacobson S. Increased HTLV-I proviral load and preferential expansion of HTLV-I tax-specific CD8+ T cells in cerebrospinal fluid from patients with HAM/TSP. Ann Neurol 2001a; 50: 807–12.

Nagai M, Brennan MB, Sakai JA, Mora CA, Jacobson S. CD8(+) T cells are an *in vivo* reservoir for human T-cell lymphotropic virus type I. Blood 2001b; 98: 1858–61.

Nagai M, Usuku K, Matsumoto W, Kodama D, Takenouchi N, Moritoyo T, et al. Analysis of HTLV-I proviral load in 202 HAM/TSP patients and 243 asymptomatic HTLV-I carriers: high proviral load strongly predisposes to HAM/TSP. J Neurovirol 1998; 4: 586–93.

Narikawa K, Fujihara K, Misu T, Feng J, Fujimori J, Nakashima I, et al. CSF-chemokines in HTLV-I-associated myelopathy: CXCL10 up-regulation and therapeutic effect of interferon-alpha. J Neuroimmunol 2005; 159: 177–82.

Nie CQ, Bernard NJ, Norman MU, Amante FH, Lundie RJ, Crabb BS, et al. IP-10-mediated T cell homing promotes cerebral inflammation over splenic immunity to malaria infection. PLoS Pathog 2009; 5: e1000369.

Osame M. Review of WHO kagoshima meeting and diagnostic guidelines for HAM/TSP. In: Blattner WA, editor. Human retrovirology: HTLV. New York: Raven Press, 1990. p. 191–7.

Osame M, Usuku K, Izumo S, Ijichi N, Amitani H, Igata A, et al. HTLV-I associated myelopathy, a new clinical entity. Lancet 1986; 1: 1031–2.

Proost P, Vynckier AK, Mahieu F, Put W, Grillet B, Struyf S, et al. Microbial toll-like receptor ligands differentially regulate CXCL10/IP-10 expression in fibroblasts and mononuclear leukocytes in synergy with IFN-gamma and provide a mechanism for enhanced synovial chemokine levels in septic arthritis. Eur J Immunol 2003; 33: 3146–53.

Proost P, Schutyser E, Menten P, Struyf S, Wuyts A, Opdenakker G, et al. Amino-terminal truncation of CXCR3 agonists impairs receptor signaling and lymphocyte chemotaxis, while preserving antiangiogenic properties. Blood 2001; 98: 3554–61.

Qin S, Rottman JB, Myers P, Kassam N, Weinblatt M, Loetscher M, et al. The chemokine receptors CXCR3 and CCR5 mark subsets of T cells associated with certain inflammatory reactions. J Clin Invest 1998; 101: 746–54.

Randall RE, Goodbourn S. Interferons and viruses: an interplay between induction, signalling, antiviral responses and virus countermeasures. J Gen Virol 2008; 89: 1–47.

Richardson JH, Edwards AJ, Cruickshank JK, Rudge P, Dalgleish AG. *In vivo* cellular tropism of human T-cell leukemia virus type 1. J Virol 1990; 64: 5682–7.

Saito M, Bangham CR. Immunopathogenesis of human T-cell leukemia virus type-1-associated myelopathy/tropical spastic paraparesis: recent perspectives. Leuk Res Treatment 2012; 2012: 259045.

Sallusto F, Lenig D, Mackay CR, Lanzavecchia A. Flexible programs of chemokine receptor expression on human polarized T helper 1 and 2 lymphocytes. J Exp Med 1998; 187: 875–83.

Shimoyama M. Diagnostic criteria and classification of clinical subtypes of adult T-cell leukaemia-lymphoma. A report from the lymphoma study group (1984–87). Br J Haematol 1991; 79: 428–37.

Sung JH, Zhang H, Moseman EA, Alvarez D, Iannacone M, Henrickson SE, et al. Chemokine guidance of central memory T cells is critical for antiviral recall responses in lymph nodes. Cell 2012; 150: 1249–63.

Tanaka M, Matsushita T, Tateishi T, Ochi H, Kawano Y, Mei FJ, et al. Distinct CSF cytokine/chemokine profiles in atopic myelitis and other causes of myelitis. Neurology 2008; 71: 974–81.

Tattermusch S, Skinner JA, Chaussabel D, Banchereau J, Berry MP, McNab FW, et al. Systems biology approaches reveal a specific interferon-inducible signature in HTLV-1 associated myelopathy. PLoS Pathog 2012; 8: e1002480.

Teixeira AL Jr, Cardoso F, Souza AL, Teixeira MM. Increased serum concentrations of monokine induced by interferon-gamma/CXCL9 and interferon-gamma-inducible protein 10/CXCL-10 in sydenham's chorea patients. J Neuroimmunol 2004; 150: 157–62.

Thomas SY, Hou R, Boyson JE, Means TK, Hess C, Olson DP, et al. CD1d-restricted NKT cells express a chemokine receptor profile indicative of Th1-type inflammatory homing cells. J Immunol 2003; 171: 2571–80.

Umehara F, Izumo S, Ronquillo AT, Matsumuro K, Sato E, Osame M. Cytokine expression in the spinal cord lesions in HTLV-I-associated myelopathy. J Neuropathol Exp Neurol 1994; 53: 72–7.

Van den Steen PE, Deroost K, Van Aelst I, Geurts N, Martens E, Struyf S, et al. CXCR3 determines strain susceptibility to murine cerebral malaria by mediating T lymphocyte migration toward IFN-gamma-induced chemokines. Eur J Immunol 2008; 38: 1082–95.

Waldmann TA. The biology of interleukin-2 and interleukin-15: implications for cancer therapy and vaccine design. Nat Rev Immunol 2006; 6: 595–601.

Yamano Y, Sato T. Clinical pathophysiology of human T-lymphotropic virus-type 1-associated myelopathy/tropical spastic paraparesis. Front Microbiol 2012; 3: 389.

Yamano Y, Takenouchi N, Li HC, Tomaru U, Yao K, Grant CW, et al. Virus-induced dysfunction of CD4+CD25+ T cells in patients with HTLV-I-associated neuroimmunological disease. J Clin Invest 2005; 115: 1361–8.

Yamano Y, Nagai M, Brennan M, Mora CA, Soldan SS, Tomaru U, et al. Correlation of human T-cell lymphotropic virus type 1 (HTLV-1) mRNA with proviral DNA load, virus-specific CD8(+) T cells, and disease severity in HTLV-1-associated myelopathy (HAM/TSP). Blood 2002; 99: 88–94.

Yamano Y, Araya N, Sato T, Utsunomiya A, Azakami K, Hasegawa D, et al. Abnormally high levels of virus-infected IFN-gamma+ CCR4+ CD4+ CD25+ T cells in a retrovirus-associated neuroinflammatory disorder. PLoS One 2009; 4: e6517.

Yasuda N, Lai PK, Ip SH, Kung PC, Hinuma Y, Matsuoka M, et al. Soluble interleukin 2 receptors in sera of japanese patients with adult T cell leukemia mark activity of disease. Blood 1988; 71: 1021–6.

blood

2013 121: 4340-4347
Prepublished online March 28, 2013;
doi:10.1182/blood-2012-08-446922

Preapoptotic protease calpain-2 is frequently suppressed in adult T-cell leukemia

Makoto Ishihara, Natsumi Araya, Tomoo Sato, Ayako Tatsuguchi, Naomi Saichi, Atae Utsunomiya, Yusuke Nakamura, Hidewaki Nakagawa, Yoshihisa Yamano and Koji Ueda

Blood (print ISSN 0006-4971, online ISSN 1528-0020), is published weekly by the American Society of Hematology, 2021 L St, NW, Suite 900, Washington DC 20036.

Regular Article

LYMPHOID NEOPLASIA

Preapoptotic protease calpain-2 is frequently suppressed in adult T-cell leukemia

Makoto Ishihara,[1] Natsumi Araya,[2] Tomoo Sato,[2] Ayako Tatsuguchi,[1] Naomi Saichi,[1] Atae Utsunomiya,[3] Yusuke Nakamura,[4] Hidewaki Nakagawa,[1] Yoshihisa Yamano,[2] and Koji Ueda[1]

[1]Laboratory for Biomarker Development, Center of Genomic Medicine, RIKEN, Tokyo, Japan; [2]Department of Molecular Medical Science, Institute of Medical Science, St. Marianna University School of Medicine, Kawasaki, Japan; [3]Department of Hematology, Imamura Bun-in Hospital, Kagoshima, Japan; and [4]Section of Hematology/Oncology, Department of Medicine Faculty, The University of Chicago, Chicago, IL

Key Points

- Proteome-wide analysis of HTLV-1–infected T cells identified 17 biomarker proteins for the diagnosis of ATL or HAM/TSP patients.

Adult T-cell leukemia (ATL) is one of the most aggressive hematologic malignancies caused by human T-lymphotropic virus type 1 (HTLV-1) infection. The prognosis of ATL is extremely poor; however, effective strategies for diagnosis and treatment have not been established. To identify novel therapeutic targets and diagnostic markers for ATL, we employed focused proteomic profiling of the $CD4^+CD25^+CCR4^+$ T-cell subpopulation in which HTLV-1–infected cells were enriched. Comprehensive quantification of 14 064 peptides and subsequent 2-step statistical analysis using 29 cases (6 uninfected controls, 5 asymptomatic carriers, 9 HTLV-1–associated myelopathy/tropical spastic paraparesis patients, 9 ATL patients) identified 91 peptide determinants that statistically classified 4 clinical groups with an accuracy rate of 92.2% by cross-validation test. Among the identified 17 classifier proteins, α-II spectrin was drastically accumulated in infected T cells derived from ATL patients, whereas its digestive protease calpain-2 (CAN2) was significantly downregulated. Further cell cycle analysis and cell growth assay revealed that rescue of CAN2 activity by overexpressing constitutively active CAN2 (Δ_{19}CAN2) could induce remarkable cell death on ATL cells accompanied by reduction of α-II spectrin. These results support that proteomic profiling of HTLV-1–infected T cells could provide potential diagnostic biomarkers and an attractive resource of therapeutic targets for ATL. (*Blood.* 2013;121(21):4340-4347)

Introduction

Human T-lymphotropic virus type 1 (HTLV-1) is a human retrovirus that is the pathogenic agent of HTLV-1–associated diseases, such as adult T-cell leukemia (ATL) and HTLV-1–associated myelopathy/tropical spastic paraparesis (HAM/TSP). Recent epidemiological studies revealed that HTLV-1 is endemic mainly in Japan, the Caribbean basin, Iran, Africa, South America, and the Melanesian islands.[1] Other estimates have shown that 20 million to 30 million people worldwide are infected with HTLV-1.[2] The infection is followed by a prolonged asymptomatic phase of 20 to 30 years, and 2% to 5% of the infected individuals develop ATL during their lifetime.[3] ATL is one of the most aggressive hematologic malignancies characterized by increased numbers of lymphocytes with multilobulated nuclei, so-called flower cells, in blood circulation. The prognosis is severe with the median overall survival period and 5-year survival rate of ATL patients of 7 months and 20%, respectively.[4] Recently, humanized anti-CCR4 (KW-0761) therapeutic antibody achieved a great improvement in ATL treatment in a phase 3 study. However, the disease control rate was restricted to 50%, and long-term prognosis has yet to be known.[5] For future improvements in the management of ATL, novel biomarkers for early diagnosis are urgently needed for early therapeutic intervention.

To date, comprehensive genomic or proteomic studies using $CD4^+$ T cells have been performed for this purpose,[6-9] but reproducibility and reliability of quantification results in the discovery phase were uncertain due to the diverse individual variety of HTLV-1–infected cell contents in $CD4^+$ T cells. To overcome the etiologic variety of samples, we focused on the $CD4^+CD25^+CCR4^+$ T-cell subpopulation since Yamano et al[10] recently revealed that HTLV-1 preferentially infected $CD4^+CD25^+CCR4^+$ T cells in both ATL and HAM/TSP patients. By targeting $CD4^+CD25^+CCR4^+$ T cells, we here provide the first quantitative proteome map illustrating molecular disorders in pathogenic human T cells directly associated with the onset or progression of ATL. The comprehensive and comparative interpretation of total proteome in infected cells, especially between asymptomatic HTLV-1 carriers and ATL patients, could immediately lead to specific candidates for biomarkers and drugs.

Another challenge to emphasize in this study is our recently established proteomic profiling technologies. It is indisputable that the greater the number of clinical samples analyzed, the more confidently statistical analysis can be undertaken in order to identify diagnostic markers and druggable targets. Despite this fact, previous proteomics reports could not provide high-throughput quantitative methodologies that were sufficient for dealing with even more than 10 clinical samples, excepting a study utilizing a surface enhanced laser desorption/ionization time of flight mass spectrometer. Although the surface enhanced laser desorption/ionization time of flight method drastically improved the performance in both quantification and throughput, allowing relative quantification

Submitted August 1, 2012; accepted March 25, 2013. Prepublished online as *Blood* First Edition paper, March 28, 2013; DOI 10.1182/blood-2012-08-446922.

The online version of this article contains a data supplement.

The publication costs of this article were defrayed in part by page charge payment. Therefore, and solely to indicate this fact, this article is hereby marked "advertisement" in accordance with 18 USC section 1734.

analysis for 96 samples in several hours, at most only 250 unidentified protein peaks were detectable. In the present study, we integrated the proteomics server for the huge data set "Expressionist" (Genedata A.G., Basel, Switzerland) with high-end mass spectrometers to maximize the quality and quantity of protein catalogs transferred from mass spectrometers. We first describe the discovery phase providing a panel of novel diagnostic molecules from quantification of 14 064 peptides and identification of 4763 proteins. As the functional validation phase, we further examined the physiological potential of an identified diagnostic marker candidate, calpain-2 (CAN2), particularly concerning the association of its activity with survival or progression of ATL cells.

Materials and methods

PBMCs and cell lines

Peripheral blood mononuclear cells (PBMCs) from 6 normal donors, 5 asymptomatic carriers, and 9 HAM/TSP patients used in the screening analysis were collected in the St. Marianna University School of Medicine. Those from 9 ATL patients were collected in the Imamura Bun-in Hospital. PBMCs from 4 ATL patients used for the validation experiments were provided by the Joint Study on Predisposing Factors of ATL Development. The others from 4 HAM/TSP patients were collected in the St. Marianna University School of Medicine. The use of these human specimens in this study was approved by individual institutional ethical committees: the Ethical Committee of Yokohama Institute, RIKEN (approval code Yokohama H22-3); the Ethical Committee of St. Marianna University School of Medicine; the Institutional Review Board of Imamura Bun-in Hospital; and the Ethical Committee of the University of Tokyo (approval code 10-50). This study was conducted in accordance with the Declaration of Helsinki.

SO-4, KOB, and KK1 cells were kindly provided by Dr Yasuaki Yamada, cultured in RPMI 1640 supplemented with 10% fetal bovine serum (Cell Culture Bioscience, Tokyo, Japan), 100 kU/L interleukin 2 (Cell Science & Technology Institute Inc., Tokyo, Japan), and 1 × antibiotic-antimycotic solution (Sigma-Aldrich, MO). Jurkat, SUP-T1, CCRF-CEM, and MOLT-3 cells were cultured in RPMI 1640 supplemented with 10% fetal bovine serum and 1 × antibiotic-antimycotic solution. All cell lines were grown at 37°C in 5% CO_2. $CD3^+CD4^+CD25^+CCR4^+$ T cells were isolated with anti-CD3-FITC (eBioscience, San Diego, CA), anti-CCR4-PE (Becton Dickinson, CA), anti-CD4-Cy7 (eBioscience), and anti-CD25-APC (eBioscience) on a Cell Sorter JSAN (Bay Bioscience, Hyogo, Japan).

Sample preparation for mass spectrometric analysis

The $CD4^+CD25^+CCR4^+$ T cells were washed with phosphate-buffered saline 3 times and lysed in denaturation buffer (8 M urea in 50 mM ammonium bicarbonate). After sonication, reduction with 5 mM tris(2-carboxyethyl) phosphine (Sigma-Aldrich) at 37°C for 30 minutes, and alkylation with 25 mM iodacetamide (Sigma-Aldrich) at room temperature for 45 minutes, lysates were digested with Trypsin GOLD (Promega, WI) with protein/enzyme ratio of 25:1 at 37°C for 12 hours. The digested peptides were desalted with Oasis HLB μElution plate (Waters, MA). The collected samples were dried up with a Vacuum Spin Drier (TAITEC Co. Ltd., Saitama, Japan) and subjected to mass spectrometric analyses.

Liquid chromatography tandem mass spectrometry (LC/MS/MS)

The digested peptides were separated on a 0.1 × 200 mm homemade C_{18} column using a 2-step linear gradient, 2% to 35% acetonitrile for 95 minutes and 35% to 95% acetonitrile for 15 minutes in 0.1% formic acid with a flow rate of 200 nL/min. The eluting peptides were analyzed with a QSTAR-Elite mass spectrometer (AB Sciex, CA) in the smart information-dependent acquisition mode of Analyst QS software 2.0 (AB Sciex). The other parameters on QSTAR-Elite were shown as follows: DP = 60, FP = 265, DP2 = 15, CAD = 5, IRD = 6, IRW = 5, curtain gas = 20, and ion spray voltage = 2000 V.

Two-dimensional (2D) LC/MS/MS

Tryptic digests of $CD4^+CD25^+CCR4^+$ T cells were dissolved in 10 mM ammonium formate in 25% acetonitrile and fractionated by a 0.2 × 250 mm monolith strong cation exchange column (GL Science, Tokyo, Japan). Peptides were eluted with an ammonium formate gradient from 10 mM to 1 M in curve = 3 mode for 70 minutes using a Prominence high-performance liquid chromatography (HPLC) system (Shimadzu Corporation, Kyoto, Japan). The eluate was fractionated into 20 fractions and analyzed individually by LTQ-Orbitrap-Velos mass spectrometer (Thermo Scientific, Bremen, Germany) accompanied with the Ultimate 3000 nano-HPLC system. The fractionated peptide samples were separated with the same gradient used in the QSTAR-Elite system described previously and analyzed by LTQ-Orbitrap-Velos acquiring a full MS scan on Fourier-transition mode with MS resolution = 60 000 and simultaneously MS/MS scans for the 20 most intense precursor ions in each MS spectrum on ion-trap mode with regular resolution. Other important parameters for LTQ-Orbitrap-Velos were as follows: capillary temp = 250, source voltage = 2 kV, MS scan range = mass-to-charge ratio (m/z) 400 to 1600, acquire data dependent CID MS/MS for top-20 intense precursors, and dynamic exclusion enabled during 30 seconds. For protein identification, all MS/MS spectra were searched against SwissProt database version 2012_06 (20 232 human protein sequences) using SEQUEST algorithm on ProteomeDiscoverer 1.3 software (Thermo Scientific) with the following parameters: MS tolerance = 3 ppm, MS/MS tolerance = 0.8 Da, maximum missed cleavages = 2, enzyme = trypsin, taxonomy = *Homo sapiens*, fixed modification = carbamidomethylation on cysteine, and variable modification = oxidation on methionine. We accepted the protein identification satisfying the false discovery rate <1% by Percolator false discovery rate estimation algorithm on ProteomeDiscoverer.

Label-free quantification analysis

The LC/MS/MS raw data were imported into the Expressionist RefinerMS module and subjected to the following data processing and relative quantification steps. The total work flow on the RefinerMS module is shown in supplemental Figure 1 (see the *Blood* Web site). The LC/MS/MS raw data set from 29 clinical samples was displayed in 2D planes (m/z vs retention time [RT]). The chromatogram grid was applied to all planes: scan counts = 10, polynom order = 3, and RT smoothing = 0. The planes were simplified by subtracting background noises using chromatogram chemical noise subtraction: RT window = 50 scans, quantile subtraction = 50%, and RT smoothing = 3 scans. After the noise subtraction, data points with intensity <10 were clipped to zero. The RT variety among 29 planes was adjusted by chromatogram RT alignment: RT transformation window = 0.2 minutes, RT search interval = 5 minutes, m/z window = 0.1 Da, and gap penalty = 1. Peaks were detected by chromatogram summed peak detection: summation window = 5 scans, overlap = 50, minimum peak size = 4 scans, maximum merge distance = 10 points, peak RT splitting = true, intensity profiling = max, gap/peak ratio = 1%, refinement threshold = 5, consistency threshold = 0.8, and signal/noise threshold = 1. The detected peaks were grouped into isotopic clusters derived from each molecule using 2-step chromatogram isotopic peak clustering. The first parameters were as follows: minimum charge = 1, maximum charge = 10, maximum missing peaks = 0, first allowed gap position = 3, RT window = 0.1 minute, m/z tolerance = 0.05 Da, isotope shape tolerance = 10, and minimum cluster size ration = 1.2. The second parameters were as follows: minimum charge = 1, maximum charge = 10, maximum missing peaks = 0, first allowed gap position = 3, RT window = 0.1 minute, m/z tolerance = 0.05 Da, and minimum cluster size ration = 0.6.

Expression vectors and siRNA

For the Δ_{19}CAN2 construct, the *CAPN2* fragment was amplified with primers 5′-CATGTCGACTCCCACGAGAGGGCCATCAAGT-3′ and 5′-CATTC-TAGATCAAAGTACTGAGAAACAGAGCC-3′ from pBlueBacIII *CAPN2* and cloned into pEFBOS-Myc. Prior to the overexpression experiments, we confirmed that the sequence of the inserted *CAPN2* fragment was identical to the Mammalian Gene Collection sequence (accession number

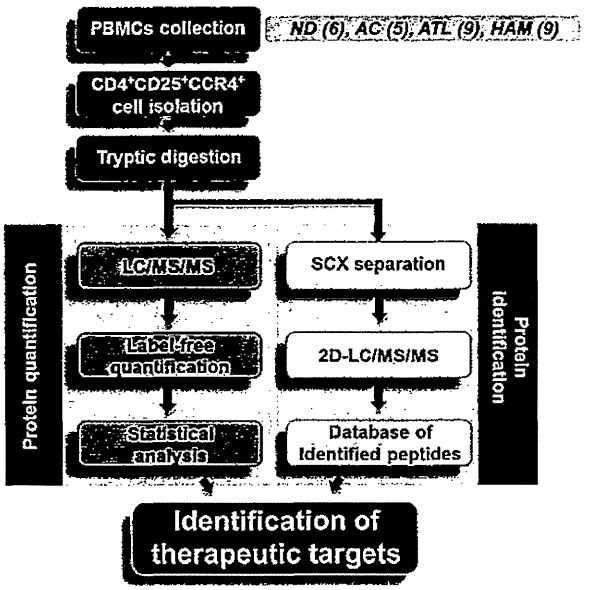

Figure 1. Schematic overview of proteomic profiling for $CD4^+CD25^+CCR4^+$ cells. PBMCs were collected from 6 normal donors, 5 asymptomatic carriers, 9 ATL patients, and 9 HAM/TSP patients, followed by isolation of the $CD4^+CD25^+CCR4^+$ subset using the cell-sorting system. The statistical candidate selection steps, including LC/MS/MS data processing, label-free quantification, and statistical analysis, were performed on the Expressionist proteome server. The protein identification database was separately established based on 2D LC/MS/MS analysis. ND, normal donors; AC, asymptomatic carriers.

BC021303). The 5-μg vector DNA was transfected to 1×10^6 cells. The small interfering RNAs (siRNAs) against *SPTAN1*, *PTMS*, *HSPE1*, and SHMT2 and siRNA universal negative control were purchased from Sigma-Aldrich. The 500-pmol siRNA oligo was transfected into 1×10^6 cells. The vectors and siRNAs were transfected into all cell lines except CCRF-CEM by Amaxa Nucleoportator transfection Kit V (Lonza, Cologne, Germany) and CCRF-CEM by Kit C (Lonza).

Cell cycle analysis and proliferation assay

For the cell cycle analysis, 1×10^5 to 2×10^5 cells were washed and agitated in 0.1% Triton-X (Sigma-Aldrich) with 100 ng/mL of ribonuclease (Sigma-Aldrich). Following addition of 1 μg/mL propidium iodide, the flow cytometric analysis was performed on FACScalibur (Becton Dickinson). The data analysis was performed using FlowJo software (Tree Star Inc., OR). Doublet events were eliminated from analyses by proper gating on FL2-W/FL2-A primary plots before histogram analysis of DNA content. Cell proliferation was estimated by measuring cell metabolic activity using Cell Counting Kit-8 (Dojindo, Kumamoto, Japan) following the manufacturer's recommendation.

Western blotting

Cells were lysed in lysis buffer [1% NP-40, 2 mM EGTA, 2 mM $MgCl_2$, 150 mM NaCl, 20 mM tris(hydroxymethyl)aminomethane–HCl (pH 7.5), 10% glycerol, containing the protease inhibitor cocktail Complete (Roche, IN)] and subjected to sodium dodecyl sulfate–polyacrylamide gel electrophoresis and transferred onto PVDF membranes. Following blocking with 4% Block Ace (Yukijirushi Nyugyo Inc., Tokyo, Japan), membranes were incubated with anti-myc (9E10; Sigma-Aldrich) or anti–α-II spectrin (Abcam, Cambridge, UK) antibodies. Membranes were then incubated with horseradish peroxidase–conjugated anti-mouse IgG (GE Healthcare, NJ) or anti-rabbit IgG (GE Healthcare), respectively, and visualized with Western Lightning kit (Perkin Elmer, MA).

Multiple reaction monitoring (MRM)

$CD4^+$ T cells were isolated from PBMCs using flow cytometry. The tryptic digests of the isolated cells were analyzed by 4000 Q-TRAP mass spectrometer (AB Sciex) accompanied with Ultimate 3000 nano-HPLC system. The LC gradient was as follows: 2% to 30% acetonitrile for 10 minutes and 30% to 95% acetonitrile for 5 minutes in 0.1% formic acid with a flow rate of 300 nL/min. The MRM transitions monitored were m/z 409.7/375.2 for α-II spectrin (SPTA2); m/z 538.3/889.5 for parathymosin (PTMS); m/z 507.3/147.1 for heat shock 10-kDa protein, mitochondrial (CH10); m/z 490.3/147.1 for serine hydroxymethyltransferase, mitochondrial (GLYM); and m/z 581.3/919.5 for β-actin, respectively. Individual peak areas were normalized by the peak area of β-actin. Data acquisition was performed with ion spray voltage = 2300 V, curtain gas = 10 psi, nebulizer gas = 10 psi, and an interface heating temperature = 150°C. The parameters were set as follows: declustering potential = 60, entrance potential = 10, collision cell exit potential = 10, and dwell time for each transition = 10 seconds. Collision energy was optimized to achieve maximum intensity for each MRM transition as follows: 34.03 V for m/z 409.7/175.1, 24.68 eV for m/z 538.3/889.5, 23.32 eV for m/z 507.3/147.1, 37.57 eV for m/z 490.3/147.1, and 31.58 eV for m/z 581.3/919.5.

Results

Quantitative proteome profiling of $CD4^+CD25^+CCR4^+$ T cells

A schematic overview of the screening approach is shown in Figure 1. To identify diagnostic markers expressed in HTLV-1–infected T cells, a $CD4^+CD25^+CCR4^+$ subset of PBMCs from 6 uninfected volunteers, 5 asymptomatic carriers, 9 HAM/TSP patients, and 9 ATL patients was isolated by flow cytometry (Figure 2). The averaged proportion of $CD4^+CD25^+CCR4^+$ cells in $CD4^+$ T cells from 4 clinical groups was 6.48 ± 2.46%, 13.17 ± 13.06%, 20.55 ± 10.73%, and 55.83 ± 22.40%, respectively, indicating that the occupancy of viral reservoir cells varied drastically among both pathological groups and even individuals within a group. Enrichment of the infected cells was confirmed by viral load measurement of the used samples (supplemental Figure 2). As reported previously,[10] the viral load of $CD4^+CD25^+CCR4^+$ cells (37.91 copies/100 cells on average) was ~10 times higher than that of $CD4^+CD25^-CCR4^-$ cells (4.12 copies/100 cells on average), indicating that the former cells were evidently the HTLV-1–enriched fraction. This fact strongly supports the importance of

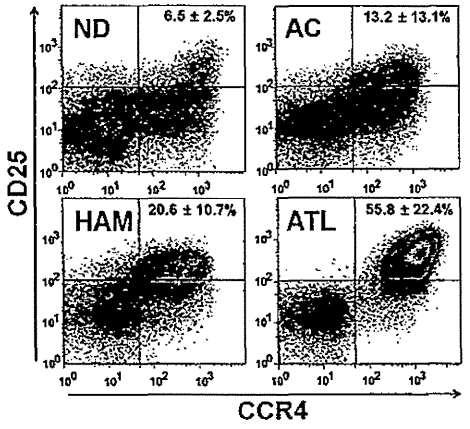

Figure 2. Representative sorting results of $CD4^+CD25^+CCR4^+$ cells. After labeling with anti-CD3-FITC, anti-CD4-Cy7, anti-CD25-APC, and anti-CCR4-PE, the $CD3^+CD4^+CD25^+CCR4^+$ fraction was isolated. The averaged content ± standard deviation (%) of $CD25^+CCR4^+$ cells out of $CD3^+CD4^+$ cells was calculated for each clinical group and is displayed in the upper right section of the panels.

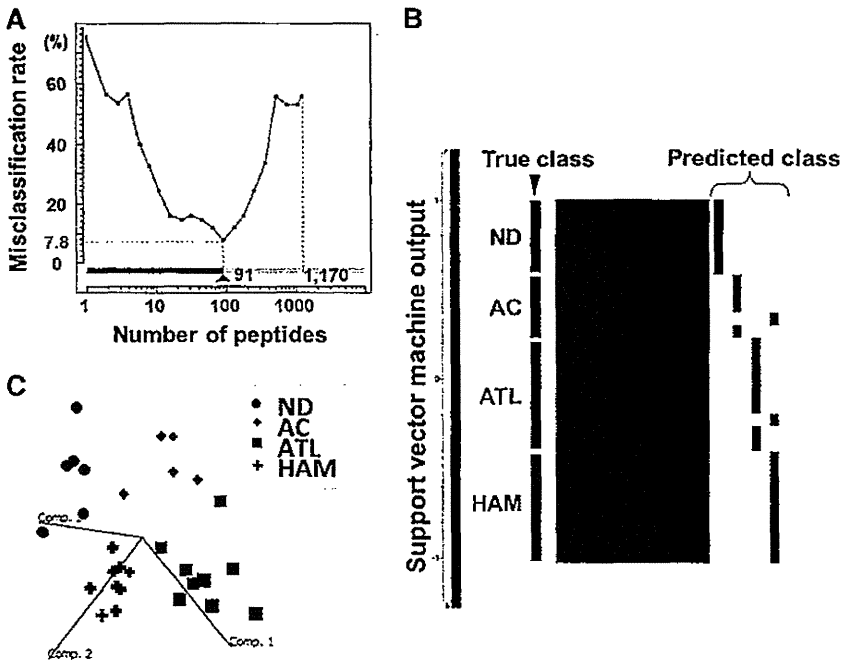

Figure 3. Statistical extraction of candidate therapeutic targets. The 14 064 nonredundant peptides detected were subjected to a 4-group Kruskal-Wallis test (ND, AC, ATL, and HAM), resulting in identification of 1170 first candidates ($P < .01$). ND, normal donors; AC, asymptomatic carriers. (A) Next, the Expressionist ranking method further narrowed down the candidates to 91 peptides based on SVM-REF so that the misclassification rate in the cross-validation test became minimum, 7.8%. (B) The predicted classification result by leave-one-out cross-validation test. The 27 out of 29 cases were successfully classified into the true classes. (C) The three-dimensional plot shows the additional assessment for the classification power of 91 classifiers by principal component analysis. Comp. 1 to 3 indicate principal components 1 to 3.

enriching pathogenic cells for rigorous quantitative biomarker discovery.

An accurately adjusted number of $CD4^+CD25^+CCR4^+$ cells from 29 cases were digested with trypsin and subjected to LC/MS/MS analysis individually. Because recent mass spectrometers often deal with data on the order of hundreds of megabytes per sample, it has been considered almost impossible to calculate a data set larger than a gigabyte from large-scale clinical samples on desktop computers. Hence, we constructed a proteomics server equipped with a 12-core central processing unit, 36 SAS hard disks, and 192-GB physical memories driving the Expressionist, which was designed to combine the database module, the data processing module, and the statistical analysis module into a single integrative platform for genomics, proteomics, and metabolomics. The detailed work flow for data processing and quantification for 29 LC/MS/MS raw data was described in the "Materials and methods" and is illustrated in supplemental Figure 1. Finally, 68 454 nonredundant peaks were detected and grouped into 37 143 isotopic clusters, or molecules. As tryptic peptides should appear as multivalent ions in electrospray ionization mass spectra, 23 079 singly charged ions were removed, resulting in utilization of 14 064 peptide signals for further statistical selection of diagnostic markers.

Statistical identification of candidate diagnostic markers for ATL

A stepwise statistical extraction was employed for the effective identification of proteins, which demonstrated specific up- or downregulation in the ATL group. In the first stage, a 4-group Kruskal-Wallis test was performed to roughly extract the candidates showing a significantly distinct expression level among 4 clinical groups. Here we set the cutoff line at $P < .01$ and obtained 1170 first candidate peptides simply because the isolated peptide set using this criterion showed the best performance in the following prediction model.

Next, we selected the final candidates by the support vector machine–recursive feature elimination algorithm in the Expressionist Analyst module. Support vector machine–recursive feature elimination is a candidate elimination method based on SVM, which enabled us to improve the classification outputs by selecting the best-performing peptide set among initially provided candidates.[11] As a result, a combination of 91 peptides showed the lowest misclassification rate (7.78%) in a leave-one-out cross-validation test (Figure 3A-B). To evaluate the classification efficiency of 91 selected candidates, the principal component analysis was performed. Figure 3C shows the three-dimensional plot of 29 clinical samples based on the 3 best-explainable components, which illustrated statistically clear segregation among the 4 clinical groups. These assessments indicated that the 91 peptides should be a sufficient set of classifiers that closely associated with the pathological characteristics of the 4 clinical groups.

Based on an independently constructed 6279-protein identification database for $CD4^+CD25^+CCR4^+$ cells using 2D LC/MS/MS (see details in "Materials and methods"), 19 peptides among the 91 candidate peptides were successfully assigned to 17 proteins listed in Table 1. The mass spectrometric quantification profiles for the 19 peptides are also shown in Figure 4 (box plots).

Recovering CAN2 activity induced cell death in ATL cells

Our diagnostic marker discovery for ATL identified an enzyme-substrate pair, CAN2 and SPTA2, which demonstrated significantly aberrant expression level in ATL patients (Figure 4). Interestingly, the intensities of the 2 proteins in 27 screening cases (without 2 statistical outliers in Figure 4) showed a clearly inverse correlation ($R^2 = 0.395$, Figure 5A). To examine whether CAN2 downregulation and/or SPTA2 upregulation might be essential for the growth of ATL cells, the enzymatic activity of CAN2 was rescued by overexpressing the constitutively active form of CAN2 (Δ_{19}CAN2) in 3 ATL cell lines, SO-4, KOB, and KK1. After 36 hours of transfection, significant inhibition of cell proliferation (Figure 5B) and induction of sub-G1 transition was observed by activation of CAN2 in 3 ATL cells, but not in 4 non-ATL leukemia cell lines (Figure 5C). Furthermore, overexpression of Δ_{19}CAN2 drastically attenuated the expression level of SPTA2 in the ATL cell

Table 1. List of 17 protein classifiers for categorization of normal donors, asymptomatic carriers, HAM/TSP, and ATL

Accession	Protein name	*P* value (Kruskal-Wallis test)	m/z	RT	Charge	Peptide score	Identity or homology threshold	Sequence
LPPL	Eosinophil lysophospholipase	2.3.E-03	409.722	47.4	2	36.3	27	MVQVWR
CH10	Heat shock 10-kDa protein, mitochondrial	2.5.E-03	430.721	40.6	2	26.2	21	GGIMLPEK
PRG2	Bone marrow proteoglycan	2.4.E-03	528.271	64.6	2	31.6	28	RLPFICSY
MOES	Moesin	8.1.E-04	532.253	26.8	2	46.2	29	EKEELMER
MNDA	Myeloid cell nuclear differentiation antigen	9.4.E-03	647.863	69.1	2	67.3	24	SLLAYDLGLTTK
GLYM	Serine hydroxymethyltransferase, mitochondrial	8.7.E-04	408.551	21.6	3	31.1	18	HADIVTTTTHK
PTMS	Parathymosin	9.7.E-04	453.875	17.8	3	41.2	25	AAEEEDEADPKR
TPIS	Triosephosphate isomerase	9.1.E-03	472.266	71.0	3	54.0	28	QSLGELIGTLNAAK
HSP71	Heat shock 70-kDa protein 1A/1B	9.7.E-03	563.307	65.5	3	93.8	21	IINEPTAAAIAYGLDR
CD6	T-cell differentiation antigen CD6	7.7.E-03	592.306	37.8	3	62.7	22	VLCQSLGCGTAVERPK
ANXA1	Annexin A1	4.4.E-04	612.347	61.5	3	57.0	17	RKGTDVNVFNTILTTR
ANXA6	Annexin A6	2.3.E-03	669.017	70.9	3	54.7	16	AMEGAGTDEKALIEILATR
SPTA2	Spectrin α chain, brain	5.4.E-03	409.718	28.8	2	42.7	30	EAGSVSLR
GLYM	Serine hydroxymethyltransferase, mitochondrial	1.1.E-03	428.240	57.0	2	42.8	27	SGLIFYR
DRB1s	HLA class II histocompatibility antigen, DRB1-1, 4, 10, 11, 13, 15, 16 β chain	1.0.E-02	478.216	25.8	2	55.9	25	AAVDTYCR
CAN2	Calpain-2 catalytic subunit	2.4.E-03	483.253	54.0	2	66.6	29	SDTFINLR
STAT1	Signal transducer and activator of transcription 1-α/β	7.3.E-03	486.290	21.7	2	39.1	29	KILENAQR
PRG2	Bone marrow proteoglycan	9.4.E-04	497.742	49.2	2	31.6	27	FQWVDGSR
CXCL7	Platelet basic protein	1.3.E-03	528.761	43.1	2	51.7	28	ICLDPDAPR

line SO-4 (Figure 5D), but not in the non-ATL leukemia cell line Jurkat (Figure 5E). On the other hand, an additional cell proliferation assay using siRNA against *SPTAN1* revealed that reduction of SPTA2 was not sufficient for the induction of cell death for ATL cells (supplemental Figures 3 and 4).

In addition, 3 proteins (PTMS, CH10, and GLYM) were also found to be upregulated in ATL cells. To address the roles of these proteins, a cell proliferation assay was conducted using 3 ATL cell lines treated with siRNAs against *PTMS*, *HSPE1* (gene symbol of CH10), or *SHMT2* (gene symbol of GLYM) (supplemental Figure 4). As a result, suppression of the *SHMT2* gene induced significant growth inhibition for all 3 ATL cell lines. Although si*HSPE1*-treated KOB cells showed a statistically significant decrease in cell growth rate, si*HSPE1* and si*PTMS* had only partial

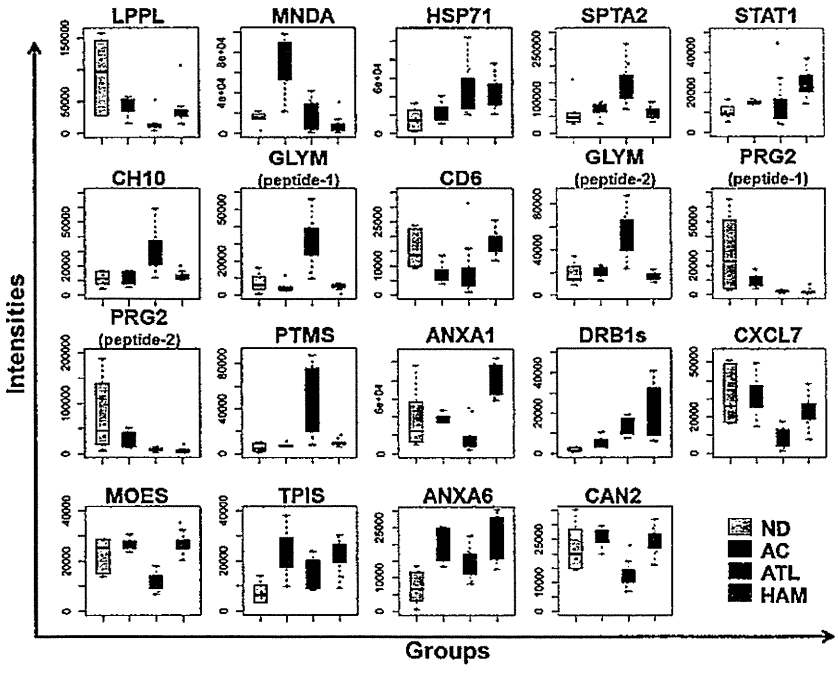

Figure 4. Summary of quantitative features for the 17 protein classifiers identified. The 19 box plots (see Table 1 for protein names) show the results of mass spectrometric quantification and protein identification. We finally identified 19 peptides out of 91 candidates in Figure 3, which were assigned to 17 proteins. Proteins identified from 2 distinct peptides were shown as GLYM (peptides 1 and 2) or PRG2 (peptides 1 and 2). The y-axis indicates normalized relative intensity of peptides in mass spectrometric data. ND, normal donors; AC, asymptomatic carriers.

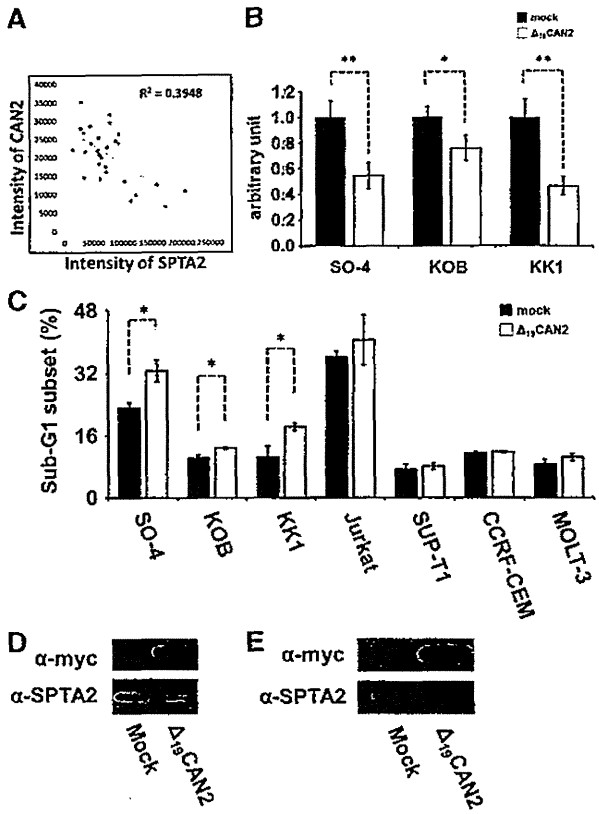

Figure 5. Rescue of CAN2 activity induced cell death in ATL cells. (A) Correlation between CAN2 and SPTA2 expression level in 27 cases. (B) Cell proliferation was measured by MTT assay on SO-4, KOB, and KK1 cells 36 hours after transfection of mock vector or Δ_{19}CAN2. $^{*}P < .05$; $^{**}P < .01$ by Student *t* test. (C) Overexpression of Δ_{19}CAN2 significantly accelerated cell death in 3 ATL (SO-4, KOB, and KK1) and 4 non-ATL (Jurkat, SUP-T1, CCRF-CEM, and MOLT-3) cell lines. $^{**}P < .05$ by Student *t* test. The drastic attenuation of SPTA2 expression was observed after transfection of Δ_{19}CAN2 in SO-4 cells (D), but not in Jurkat cells (E). The immunoblot of anti-myc tag confirmed the expression of exogenous Δ_{19}CAN2.

or no effects on proliferation of ATL cell lines. To further confirm whether the overexpression of SPTA2, PTMS, CH10, or GLYM protein would be an ATL-specific molecular signature, the expression levels of these proteins in 8 clinical samples were evaluated by the mass spectrometric quantification technology MRM (supplemental Figures 5 and 6). Expression of SPTA2, GLYM, and CH10 in cells derived from ATL patients was significantly higher than that in cells derived from HAM/TSP patients. The level of PTMS also showed a clearly increasing tendency in the ATL patient group. Taken together, these results suggested that the deprivation of CAN2 activity and upregulation of GLYM in HTLV-1–infected T cells might have a key role at the onset or progression of ATL.

Discussion

In the past decade, proteomics technologies have developed dramatically for the purpose of obtaining more and more comprehensive and sensitive proteome maps in cells or clinical specimens. The performance of mass spectrometers in particular has exhibited remarkable progress; however, as for sensitivity and throughput, it has still been difficult to identify biomarkers from crude samples including body fluids or total cell lysate. A major reason could be that the range of protein concentration in the analyte is indeed much larger than the dynamic range of recent mass spectrometers.[12] The other essential factor to be improved for clinical proteomics is the capacity of the bioinformatics platform to allow analysis of a sufficient number of clinical samples in order to statistically overcome the significant individual variability.[13]

Concerning the first issue, we previously developed and applied various focused proteomic applications targeting molecular biochemical features including glycan structure biomarkers[14-16] and low-molecular-weight peptide biomarkers.[17] The preenrichment of subproteome fractions effectively reduces the complexity of crude samples and allowed us to identify potential serum cancer biomarkers successfully. Through our previous knowledge, we provide an approach for investigating infectious diseases by employing virus-infected cell-focused proteomics. In addition to HTLV-1, for instance, isolation of HIV-infected cells is highly desired because the frequency of these cells in AIDS patients' PBMCs is ~1 out of 10^4 to 10^5 cells.[18] Actually, we successfully demonstrated the effect of HTLV-1–infected cell isolation on the elimination of individual variability (Figure 2, supplemental Figure 2) and reliable identification of disease state–associated proteins (Figures 4 and 5). We further showed the potential of the next-generation bioinformatics platform Expressionist to remove the constraint on the capacity of data size acquired from high-end mass spectrometers. Expressionist covered whole discovery steps from processing of raw mass spectrometer data to statistical analyses (Figures 1 and 3, and supplemental Figure 1) and, importantly, could perform quantification analysis using a basically unlimited number of clinical samples. Hence, in parallel with the development of mass spectrometers, high-specification and inexpensive OMICS server systems are necessary for future diagnostic marker and therapeutic target discoveries using hundreds or thousands of clinical specimens.

In this study, we focused on the $CD4^+CD25^+CCR4^+$ T-cell subpopulation in which T helper 2, T helper 17, and regulatory T (Treg) cells were mainly involved.[10] The purpose for which we used this subset was to technically enrich the preferential viral reservoir cells and to strengthen reliability of screening results. However, investigating proteome behaviors of these subtypes in HTLV-1–associated diseases is also important physiologically because it has been frequently reported that deregulated Treg plays significant roles in pathogenesis of ATL and HAM/TSP. Indeed, aberrant proliferation of Treg cells is considered the main cause of immunodeficiency in ATL patients because of their innate immunosuppressive functions,[19] whereas abnormal production of interferon γ from infected Treg cells might induce chronic spinal inflammation in HAM/TSP patients.[20] Given the list of our 17 classifier proteins, activation of signal transducer and activator of transcription 1-α/β is the well-known key factor for HAM/TSP,[21] whereas upregulation of heat shock 70-kDa protein 1A/1B, CH10, and PTMS were reported in many other types of tumors.[22-24] The association of these 4 proteins with the etiology of HAM/TSP and ATL would be evident according to the previous work, supporting that our other candidates might similarly have a direct impact on the transformation of Treg cells after infection of HTLV-1. Particularly, the specific upregulation of GLYM in ATL cells represents the first evidence that excessive folate metabolism might be essential for the progression or survival of ATL cells because GLYM is a fundamental enzyme catalyzing the supply of glycine accompanying the conversion of tetrahydrofolate to 5,10-methylenetetrahydrofolate.[25] Indeed, the suppression of GLYM expression, which was confirmed to be upregulated in ATL patients, resulted in significant reduction of cell growth. This observation suggests that diminishing GLYM